Dynamic modelling, simulation and theoretical performance analysis of Volatile Organic Compound (VOC) abatement systems in the pharma industry

Computers and Chemical Engineering 174 (2023) 108248

Contents lists available at ScienceDirect

Computers and Chemical Engineering

journal homepage: www.elsevier.com/locate/compchemeng

Dynamic modelling, simulation and theoretical performance analysis of Volatile Organic Compound (VOC) abatement systems in the pharma industry

Vasiliki E. Tzanakopoulou [a], Michael Pollitt [b], Daniel Castro-Rodriguez [b], Alexandra Costa [b], Dimitrios I. Gerogiorgis [a,*]

[a] Institute for Materials & Processes (IMP), School of Engineering, University of Edinburgh, EH9 3FB, UK
[b] GlaxoSmithKline (GSK), Montrose, Angus, Scotland DD10 8EA, UK

A B S T R A C T

Volatile Organic Compound (VOC) use is extremely widespread in the pharmaceutical industry, posing great risks, as potential organic gas releases are harmful to both environment and human health. Fixed-bed columns containing Activated Carbon (AC) or other adsorbents selectively remove VOCs from gas effluent streams. Nevertheless, adsorbing beds can be quickly and/or irregularly saturated, due to simultaneous and significant variations of flowrates and mixture compositions. This paper presents the development and implementation of a dynamic, non-isothermal adsorption model used for studying binary VOC mixture adsorption on industrial AC beds for a wide variety of structural and operating conditions. A scenario-based investigation of binary mixture behaviour examines (via multiple dynamic simulations, experimental corroboration and predictive formulas) the effect of key parameter changes on bed performance. Theoretical bed performance analysis (employing Glueckauf hodographs) has been employed to provide valuable insight into nonisothermal VOC capture bed operation, for both clean and used beds.

1. Introduction and motivation

Volatile Organic Compounds (VOC) are a class of solvents that exhibit low boiling points under atmospheric conditions. VOCs are traditionally employed for industrial process use; in the field of pharmaceutical manufacturing specifically, VOCs dominate upstream production processes by contributing a staggering 80–90% of the overall process mass inventory towards Active Pharmaceutical Ingredients (API) (Constable et al., 2007). During primary (upstream) pharmaceutical manufacturing, the main VOC-consuming stages are fluid-phase separations, especially extractions and distillations.

Because of their ubipr;equitous presence in industrial processes, VOC emissions are subject to tight regulations due to their harmful effects both on the environment, as photochemical smog formation precursors, and on human health, exacerbating respiratory conditions (Das et al., 2004; Xiong et al., 2021). Remarkably, VOC emissions from industrial processes contributed to ca. 40% of anthropogenic VOC emissions in the EU in 2017 (EEA, 2019). In an effort to mitigate climate impact in an era of ever-increasing environmental protection concerns, pharmaceutical industries emphasize VOC abatement and its process optimisation. Adsorption, which is less energy- and maintenance-intensive than other methods, is established practice, with activated carbon being the preferred adsorbent material for VOC capture (Giraudet et al., 2009, 2010). Nevertheless, quick and irregular bed saturation due to feed variability impedes process efficiency and increases costs, especially in case of outsourced adsorbent regeneration (this practice is widespread due to special regulatory requirements). First-principles process modelling, simulation and optimisation has a demonstrated potential to effectively guide industrial pharma decision-making (Gerogiorgis and Barton, 2009; Jolliffe and Gerogiorgis, 2015), particularly in the context of solvent recovery towards minimising environmental impact (Gerogiorgis and Jolliffe, 2015; Jolliffe and Gerogiorgis, 2017).

Adsorption is computationally demanding to accurately model, as it entails coupling isotherms with partial differential equations for mass and heat balances, but it is not a novel process. As a matter of fact, there is a vast body of literature covering experiments, process descriptions and variations (e.g. PSA, TSA etc.), comprehensive reviews and authoritative monographs (Ruthven, 1984). Despite the abundance of peer-reviewed literature, there is a relatively little amount of studies (Table 1) and data for pharmaceutically relevant, multicomponent VOC mixtures and even more so under industrially relevant conditions.

Table 1 summarises literature studies which mainly address single-component VOC experiments; some also focus on multicomponent mixtures both on an experimental and simulation level. The Langmuir Isotherm is predominantly used as the correlation of choice in most VOC

* Corresponding author.
E-mail address: D.Gerogiorgis@ed.ac.uk (D.I. Gerogiorgis).

https://doi.org/10.1016/j.compchemeng.2023.108248
Received 20 November 2022; Received in revised form 14 March 2023; Accepted 29 March 2023
Available online 30 March 2023

Nomenclature

b_i	Langmuir affinity coefficient (m^3 mol^{-1})
$b_{o,i}$	pre-exponential Langmuir constant (m^3 mol^{-1})
$C,$	component gas phase VOC concentration (mol m^{-3})
$C_{0,i}$	inlet concentration of i (mol m^{-3})
Cp_g	specific heat capacity of gas (J kg^{-1} K^{-1})
Cp_p	specific heat capacity of particle (J kg^{-1} K^{-1})
$C_{s0,i}$	adsorbed phase concentration at equilibrium with $C_{0,i}$ (mol m^{-3})
C_t	total gas phase VOC concentration (mol m^{-3})
D	bed inner diameter (m)
$D_{AB,i}$	molecular diffusivity (m^2 s^{-1})
$D_{eff,i}$	effective diffusivity of i (m^2 s^{-1})
$D_{k,i}$	Knudsen diffusivity (m^2 s^{-1})
d_{lm}	mean logarithmic column diameter (-)
d_p	particle diameter (m)
$D_{z,i}$	axial dispersion coefficient (m^2 s^{-1})
H_i	dimensionless Henry's constant of component i (-)
h_{int}	internal heat transfer coefficient (W m^{-2} K^{-1})
h_o	overall heat transfer coefficient (W m^{-2} K^{-1})
k_{eff}	effective thermal conductivity (W m^{-1} K^{-1})
k_{ew}	effective wall thermal conductivity (W m^{-1} K^{-1})
k_{ez}	effective axial thermal conductivity (W m^{-1} K^{-1})
$k_{f,i}$	effective mass transfer coefficient of component i (m s^{-1})
k_g	gas thermal conductivity (W m^{-1} K^{-1})
$k_{LDF,i}$	LDF mass transfer coefficient (s^{-1})
k_p	particle thermal conductivity (W m^{-1} K^{-1})
k_w	wall thermal conductivity (W m^{-1} K^{-1})
L	bed length (m)
M_r	molecular weight (g mol^{-1})
P	pressure (atm only in Eq. (4)) / (Pa)
p_1	Glueckauf variable for component 1 (-)
p_2	Glueckauf variable for component 2 (-)
q	adsorbed phase VOC concentration (mol m^{-3})
$q_{e,i}$	equilibrium adsorption capacity of i (mol kg^{-1})
$q_{\rho e,i}$	equilibrium adsorption capacity of i (mol m^{-3})
$q_{m,i}$	maximum adsorption capacity of material for component i (mol kg^{-1})
R	column inner radius (m)
Re_p	Reynolds number (adsorbent particle)
r_p	average pore radius ($1.1{\cdot}10^{-9}$ m)
R_p	particle radius (m)
SA	Surface area of adsorbent material (m^2 g^{-1})
Sc_i	Schmidt number of i
Sh	Sherwood number (-)
T	temperature (K)
T_{in}	inlet temperature (K)
T_w	wall temperature (K)
$t_{shock,i}$	shock breakthrough time of component i (s)
$t_{5\%,i}$	breakthrough onset time of component i (s)
$t_{95\%,i}$	breakthrough completion time of component i (s)
$t_{drt,i}$	duration of breakthrough (s)
u	interstitial velocity (m s^{-1})
V_{pore}	adsorbent pore volume ($5.7{\cdot}10^{-4}$ m^3 kg^{-1})
V_s	superficial velocity (m s^{-1})
x	wall thickness (m)
α_0	empirical mass diffusion correction factor (20)
$\Delta H_{ad,i}$	heat of adsorption (J mol^{-1})
ε_b	bulk bed porosity (-)
ε_p	particle porosity (-)
λ	Glueckauf variable of coherence equation (-)
μ	gas viscosity (Pa s)
$\mu_{RT,i}$	mean residence time of component i (s)
M	positive root of coherence equation (-)
N	negative root of coherence equation (-)
ρ_b	bed density (kg m^{-3})
ρ_g	gas density (kg m^{-3})
ρ_p	particle density (kg m^{-3})
$\Sigma\nu$	atomic diffusion volume (A: VOC, B: carrier)
τ_p	particle tortuosity (-)

adsorption studies; many of these belabour adsorbent material synthesis and properties, rather than studying the adsorption process itself. Very often, crucial simulation parameters (e.g. adsorbent particle size) are not explicitly reported in these publications. Moreover, adsorption studies on pharmaceutically relevant VOC solvents on large-scale beds are scarce, and the vast majority of experiments are conducted in laboratory-scale columns. This, combined with the lack of studies on multicomponent mixtures, highlights a gap in understanding and thus predicting the behaviour of industrially relevant pharmaceutical VOC mixtures when they undergo adsorption processes to ensure their removal from gas streams.

This paper presents an effort on multiple fronts, to address a pressing need to understand multicomponent, pharmaceutical VOC adsorption for industrial operations. Firstly, published experimental VOC breakthrough data are compiled from a multitude of papers and processed to produce a database of reliable Langmuir Isotherm parameters for dichloromethane, acetone, toluene and chloroform adsorption on activated carbon (AC). Secondly, this paper demonstrates the development and application of a dynamic, nonisothermal, VOC adsorption model to highlight the breakthrough characteristics of binary VOC mixtures, key to active pharmaceutical manufacturing operations. Thirdly, the effect of operating temperature and bed porosity is explored in an effort to improve modelling accuracy and pave the way for process optimisation. Finally, Glueckauf's Hodograph Theory is used to predict and visualise the dynamic adsorption behaviour of multicomponent mixtures when no experimental data is available. This is a method often overlooked but of significant value for industrial operations where fast first-principles-based insight is needed with limited experimental data availability.

2. Thermodynamic parameter estimation

Published parameter values of VOC adsorption are often unreliable or pertaining to isotherm curve fits different to the Langmuir model. In an effort to create a database for Langmuir Isotherm parameters ($q_{m,i}$ and b_i) for volatile organic compounds of interest (toluene, acetone, dichloromethane and chloroform) our study has focused on identifying and compiling published experimental data for single-component adsorption of these VOCs on activated carbon from multiple papers and fit them to the Langmuir Isotherm, Eq. (14), using Origin.

Fig. 1 shows the results of our fit for DCM compared to published experimental data and the published model of Talmoudi et al. (2018). The Langmuir Isotherm values obtained achieve more accurate data fit compared to the systematic over-estimation of the adsorbed amount in higher concentrations by the said model and have thus been used for all simulations in this paper for DCM. Published experimental data for toluene, acetone, dichloromethane and chloroform have been compiled from the literature and processed in the same way, to obtain the Langmuir Isotherm parameter values presented in Table 2 and Figs. 2 and 3.

Fig. 2a presents our estimated values of Langmuir Isotherm parameters for acetone. Published experimental data from acetone breakthrough experiments have been compiled from seven different papers pertaining to different types of activated carbon. The R^2 value of the fit

ranges from 0.841 to 0.999, which indicates that the Langmuir Isotherm is a good fit for most cases. Values for the Langmuir affinity coefficient do not follow a pattern for the same material but do range within two orders of magnitude amongst the seven papers while the maximum adsorption capacity decreases with increasing temperature for each material, as expected by theory (Ruthven, 1984). Fig. 2b shows our Langmuir Isotherm parameter estimations for DCM. Published experimental data from DCM breakthrough experiments have been compiled from five different papers pertaining to different types of activated carbon as adsorbent material. The R^2 of our fit ranges from 0.865 to 0.999, indicating that the Langmuir Isotherm is a good fit for most cases. Values for the Langmuir affinity coefficient do not follow a pattern for the same material but do range within one order of magnitude amongst these five papers. The maximum adsorbed amount decreases with increasing temperatures for each material, as expected from theory, while the variability of values for the Langmuir affinity coefficient can be attributed to the different microscopic properties of the adsorbent material which affects adsorbent-adsorbate interactions.

Fig. 3a shows our estimated values of Langmuir Isotherm parameters for TCM based on published experimental data of breakthrough experiments from the same paper pertaining to different types of adsorbents. Moreover, values by Chuang et al. (2003) are displayed, since they are used for simulation purposes in the present paper. The R^2 values of the fit range from 0.869 to 0.990. The maximum adsorption capacity values are in the same order of magnitude amongst the adsorbent materials while values of the Langmuir affinity coefficient do not follow a pattern for the same material but do range within one order of magnitude amongst the different adsorbents, possibly due to different microscopic properties. Further experimental data for chloroform adsorption on activated carbon is necessary for fitted values comparison. Fig. 3b

Table 1
Recent studies on pharmaceutically relevant Volatile Organic Compound (VOC) adsorption on activated carbon (AC).

N_{voc}	Multicomp.	Expt.	Sim.	VOC(s)	Adsorbent	Isotherm	$C_{0,max}$ (ppm)	L (m)	D (m)	Lit. Refs.
1	No	Yes	Yes	DCM	Activ. Carbon	Langmuir	8972	–	–	(Borkar et al., 2010)
1	No	Yes	Yes	Ethyl Acetate	Activ. Carbon	Langmuir	200,876	$6{\cdot}10^{-2}$	$1{\cdot}10^{-2}$	(Manjare et al., 2006)
2	Yes	Yes	Yes	Acetone, DCM	Activ. Carbon	Langmuir-Freundlich	8000	$1{\cdot}10^{-1}$	$1{\cdot}10^{-2}$	(Talmoudi et al., 2018)
2	No	Yes	Yes	Toluene Xylene	Activ. Carbon fibre	Sips	10,000	$1{\cdot}10^{-1}$	$2.5{\cdot}10^{-2}$	(Das et al., 2004)
2	No	Yes	Yes	DCM, 1,1,2-trichloro-l,2,2-trifluoroethane	Activ. Carbon	Langmuir, Sips, Freundlich	246,732	$1.5–2.5{\cdot}10^{-1}$	$4.2{\cdot}10^{-3}$	(Kim et al., 2002)
2	No	Yes	Yes	TCM, Carbon Tetrachloride	Activ. Carbon	Langmuir, Freundlich, DRK, BET	1250	$3{\cdot}10^{-1}$	$2.5{\cdot}10^{-2}$	(Kalender et al., 2015)
2	No	Yes	No	Acetone, Benzene	Activ. Carbon fibre Cloth	Dubinin-Ashtakhov	19,600	–	–	(Ramirez et al., 2005)
2	No	Yes	No	Toluene, Ethyl Acetate	Activ. Carbon	Langmuir, Freundlich, Sips, Toth, Redlich-Peterson	1666	$2.2{\cdot}10^{-1}$	$2.5{\cdot}10^{-2}$	(Li et al., 2021)
3	Yes	Yes	No	Acetaldehyde, Acetone, Ethyl Acetate	Activ. Carbon	Yoon-Nelson	208	$6{\cdot}10^{-1}$	$3.2{\cdot}10^{-4}$	(Yao et al., 2020)
3	No	Yes	Yes	TCM, Benzene, Carbon Tetrachloride	Activ. Carbon	Langmuir	6966	$9{\cdot}10^{-3}$	$1.5{\cdot}10^{-2}$	(Chuang et al., al., 2003)
3	No	Yes	Yes	Acetone, Ethyl Formate, DCM	Activ. Carbon	Langmuir	28,322	$2{\cdot}10^{-1}$	$4.6{\cdot}10^{-2}$	(Giraudet et al., 2009)
3	No	Yes	Yes	Acetone, Toluene, 1,2-dichloroethane	Activ. Carbon	Langmuir	41,415	$2{\cdot}10^{-1}$	$4.6{\cdot}10^{-2}$	(Pré et al., 2002)
3	No	Yes	No	MCM, DCM, TCM	Activ. Carbon	Langmuir	4000	$4–11{\cdot}10^{-2}$	$6.35{\cdot}10^{-3}$	(Lemus et al., 2012)
3	No	Yes	No	Acetone, TCM, Acetonitrile	Activ. Carbon, Activ. Carbon fibre, Sludge	Langmuir, Freundlich	7800	–	–	(Tsai et al., 2008)
3	No	Yes	No	Toluene, Methanol, Acetone	Activ. Carbon fibre	–	1263	–	–	(Meng et al., 2019)
3	No	Yes	No	DCM, TCM, Carbon Tetrachloride	Activ. Carbon	Langmuir, Freundlich, Temkin	5761	–	–	(Saleh et al., 2015)
3	No	Yes	No	Ethyl Acetate, Acetone, Ethanol	Activ. Carbon	Langmuir	197,386	–	–	(Gales et al., 2000Gales et al., 2003)
4	Yes	Yes	Yes	Acetone, Ethanol, Cyclohexane, Heptane	Activ. Carbon	Langmuir	6000	$1{\cdot}10^{-1}$	$1{\cdot}10^{-2}$	(Vuong et al., 2016)
4	No	Yes	Yes	Acetone, Benzene, TMB, Toluene	Activ. Carbon	Langmuir	1000	$1.5{\cdot}10^{-1}$	$1.52{\cdot}10^{-2}$	(Tefera et al., 2013)
4	No	Yes	No	DCM, TCM, Benzene, Carbon Tetrachloride	Activ. Carbon	Langmuir	400	–	–	(Chiang et al., 2001)
7	No	Yes	Yes	Acetone, 1,2-dichloroethane, Ethyl acetate, Ethyl alcohol, methylethyldioxolane, MEK, Toluene	Activ. Carbon	Langmuir	27,300	$2{\cdot}10^{-1}$	$4.6{\cdot}10^{-2}$	(Delage et al., 2000)
8	Yes	Yes	Yes	1, 2, 4-trimethylbenzene, 2, 2-dimethylpropylbenzene, Indane, Decane, Heptane, 2-butoxyethanol, 2-heptanone, n-butyl acetate, n-butanol	Activ. Carbon	Langmuir	250	$6.5{\cdot}10^{-1}$	$1.52{\cdot}10^{-2}$	(Tefera et al., 2014)

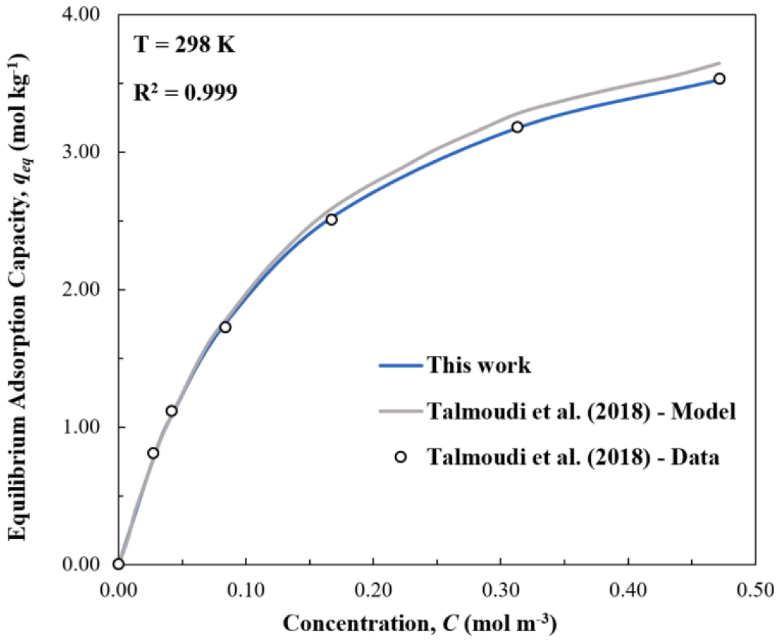

Fig. 1. Langmuir Isotherm parameter estimation for dichloromethane (DCM) (data from Talmoudi et al. 2018).

presents our estimated values of Langmuir Isotherm parameters for toluene. The experimental data come from three different papers pertaining to different types of activated carbon. The R^2 values of our fit are very high, ranging from 0.940 to 0.999, indicating the high level of accuracy that is achieved using the Langmuir Isotherm to describe toluene adsorption. Here, the maximum adsorbed amount values range within one order of magnitude amongst the three papers. Values for the Langmuir affinity coefficient for experiments conducted by Yang et al. (2018) interestingly are four orders of magnitude smaller than the other two papers, a difference attributed to the very different microscopic properties of the adsorbent materials.

3. Dynamic model development

A fixed bed, multicomponent, nonisothermal adsorption model considering mass and energy balances in the axial dimension is used to describe binary VOC mixtures adsorption. The mass transfer between the fluid and the solid phase as well as heat transfer from inside the column to the environment are described using lumped equations. The mathematical model used in this work relies on the following assumptions:

1. Radial concentration and temperature gradients are negligible (Suzuki, 1990).
2. The gas phase and adsorbent particles are in thermal equilibrium (Suzuki, 1990).
3. Wall temperature is constant and equal to the ambient temperature (Suzuki, 1990).
4. The ideal gas law applies and carrier gas adsorption is negligible (Suzuki, 1990).
5. Equilibrium obeys the Extended Langmuir model for binary mixtures (Tefera et al., 2013).

Considering all the assumptions, the overall and component mass balances are given as follows (i: component):

$$\frac{\partial C_t}{\partial t} = -\frac{\partial (uC_t)}{\partial z} - \frac{(1-\varepsilon_b)}{\varepsilon_b}\rho_p \sum \frac{\partial q_i}{\partial t} \tag{1}$$

$$\frac{\partial C_i}{\partial t} = D_{z,i}\frac{\partial^2 C_i}{\partial z^2} - \frac{\partial (uC_i)}{\partial z} - \frac{(1-\varepsilon_b)}{\varepsilon_b}\rho_p \frac{\partial q_i}{\partial t} \tag{2}$$

where C_t is the total gas phase VOC concentration, C_i is the component i gas phase *VOC* concentration, $D_{z,i}$ is the axial dispersion coefficient of component i, u is the interstitial velocity, ε_b is the bulk bed porosity, ρ_p is the particle density and q the adsorbed phase VOC concentration.

The axial dispersion coefficient of component i is given by Delgado (2006):

$$D_{z,i} = \left(\alpha_0 + \frac{Sc_i Re_p}{2}\right)\frac{D_{AB,i}}{\varepsilon_b} \tag{3}$$

where Sc_i is the Schmidt number of i, Re_p the Reynolds number (adsorbent particle), $D_{AB,i}$ the molecular diffusivity and α_0 the empirical mass diffusion correction factor.

The molecular diffusivity of component i is given by Logan (1997):

$$D_{AB,i} = 10^{-3}T^{1.75}\frac{\sqrt{\left(\frac{M_{rA}+M_{rB}}{M_{rA}M_{rB}}\right)}}{P\left((\sum v)_A^{0.33} + (\sum v)_B^{0.33}\right)^2} \tag{4}$$

where $\Sigma\nu$ is the atomic diffusion volume (A: VOC, B: carrier), T is temperature, P is pressure and M_r is the molecular weight.

Solid phase adsorption is modelled by the established Linear Driving Force (LDF) model which is characterized as "simple, analytic, and physically consistent" by Sircar et al. (2000), considering a lumped overall mass transfer coefficient (Tefera et al., 2013, 2014):

$$\frac{\partial q_i}{\partial t} = k_{LDF}\left(q_{e,i} - q_i\right) \tag{5}$$

where $k_{LDF,i}$ is the LDF mass transfer coefficient and $q_{e,i}$ is the inlet PT adsorbent equilibrium capacity.

The LDF mass transfer coefficient is given by (Tefera et al., 2013, 2014):

$$k_{LDF} = \frac{60\varepsilon_p C_{0,i} D_{eff,i}}{\tau_p C_{s0,i} d_p^2} \tag{6}$$

where ε_p is the particle porosity, $C_{0,i}$ is the inlet concentration of i, $D_{eff,i}$ is the effective diffusivity of i, τ_p is particle tortuosity, $C_{s0,i}$ is the adsorbed

Table 2
Langmuir Isotherm parameter estimation values for various adsorbents.

VOC	Authors	Adsorbent	Surf. Area ($m^2\ g^{-1}$)	T (K)	q_m (mol kg^{-1})	Standard Error	b (mol m^{-3})	Standard Error	R^2
ACT (Acetone)	(Gales et al., 2000, Gales et al., 2003)	Commercial AC	1485.00	298.00	6.173	± 0.147	1.016	± 0.137	0.986
	(Tsai et al., 2008)	Commercial AC	807.00	303.15	3.009	± 0.334	31.832	± 13.161	0.953
				323.15	2.047	± 0.520	17.960	± 13.930	0.851
				353.15	1.632	± 0.220	17.383	± 6.926	0.966
		Sludge	757.00	303.15	2.663	± 0.441	32.351	± 19.974	0.902
				323.15	1.078	± 0.072	85.182	± 27.409	0.972
				353.15	0.733	± 0.093	74.339	± 48.339	0.930
		PAN fibre	832.00	303.15	2.264	± 0.356	42.518	± 27.043	0.885
				323.15	1.786	± 0.639	11.818	± 11.166	0.787
				353.15	2.950	± 2.419	3.251	± 4.314	0.881
		Pitch fibre	1518.00	303.15	5.813	± 1.700	7.880	± 5.379	0.910
				323.15	4.458	± 1.033	3.914	± 1.606	0.983
				353.15	1.875	± 0.295	5.647	± 1.744	0.989
	(Giraudet et al., 2010)	Olive stone AC	1720.00	293.15	4.377	± 0.250	24.606	± 7.056	0.942
				313.15	3.827	± 0.215	15.581	± 3.887	0.950
				333.15	2.704	± 0.192	13.116	± 3.615	0.936
				353.15	1.127	± 0.054	29.580	± 7.476	0.925
	(Tefera et al., 2013)	Commercial AC	1390.00	298.15	7.051	± 0.023	17.311	± 0.605	0.998
	(Vuong et al., 2016)	Commercial AC	950.00	298.00	4.307	± 0.263	17.684	± 2.886	0.986
	(Talmoudi et al., 2018)	Pine AC	1706.00	298.00	6.371	± 0.213	7.677	± 0.690	0.996
				313.00	4.502	± 0.153	10.394	± 1.032	0.994
				323.00	3.617	± 0.202	8.494	± 1.280	0.988
	(Zhou et al., 2021)	Commercial AC	423.00	298.00	2.668	± 0.073	0.987	± 0.171	0.881
DCM (Dichloro-methane)	(Kim et al., 2002)	Commercial AC	826.00	303.00	6.320	± 0.186	4.188	± 0.697	0.977
				318.00	5.837	± 0.108	2.260	± 0.155	0.989
				333.00	5.299	± 0.235	1.315	± 0.209	0.968
	(Borkar et al., 2010)	Commercial AC	1000.00	303.15	4.675	± 0.143	29.471	± 4.198	0.981
				318.15	4.403	± 0.153	20.522	± 2.841	0.985
				353.15	2.619	± 0.128	12.612	± 1.698	0.989
	(Giraudet et al., 2010)	Olive stone AC	1720.00	293.15	2.448	± 0.203	24.563	± 9.756	0.885
				313.15	1.998	± 0.126	19.738	± 5.423	0.934
				333.15	1.373	± 0.071	11.402	± 1.948	0.973
				353.15	0.332	± 0.034	80.437	± 67.899	0.653
	(Lemus et al., 2012)	Commercial AC	927.00	308.15	2.905	± 0.253	29.057	± 7.138	0.953
	(Talmoudi et al., 2018)	Pine AC	1706.00	298.00	4.506	± 0.054	7.610	± 0.239	0.999
				313.00	3.332	± 0.130	8.632	± 0.921	0.994
				323.00	2.611	± 0.187	8.432	± 1.625	0.981
TCM (Chloroform)	(Tsai et al., 2008)	Commercial AC	807.00	303.15	2.826	± 0.33	119.046	± 73.188	0.890
				323.15	2.738	± 0.289	20.446	± 7.078	0.967
				353.15	2.530	± 0.325	15.277	± 5.705	0.968
		Sludge	757.00	303.15	2.213	± 0.435	21.657	± 14.487	0.868
				323.15	1.077	± 0.171	29.337	± 16.959	0.908
				353.15	0.958	± 0.110	14.268	± 4.670	0.974
		PAN fibre	832.00	303.15	2.042	± 0.098	90.631	± 21.654	0.983
				323.15	2.002	± 0.244	27.945	± 12.272	0.943
		Pitch fibre	1518.00	303.15	5.433	± 0.617	25.004	± 10.069	0.953
				323.15	4.337	± 0.354	10.414	± 2.240	0.990
				353.15	2.500	± 0.374	15.586	± 6.822	0.956
TOL (Toluene)	(Yanxu et al., 2008)	Act. Semicoke	–	293.00	0.267	± 0.002	221.795	± 23.228	0.999
	(Tefera et al., 2013)	Commercial AC	1390.00	298.15	4.525	± 0.018	366.021	± 30.724	0.939
	(Yang et al., 2018)	Wood AC 1	1284.37	303.15	3.193	± 0.286	0.064	± 0.012	0.976
		Coal AC 2	837.97	303.15	5.183	± 0.749	0.018	± 0.004	0.990
		Coal AC 3	840.03	303.15	4.352	± 0.881	0.028	± 0.009	0.943
		Coal AC 4	687.71	303.15	4.129	± 0.885	0.020	± 0.006	0.974
		Coconut AC 5	570.72	303.15	1.680	± 0.290	0.033	± 0.010	0.965

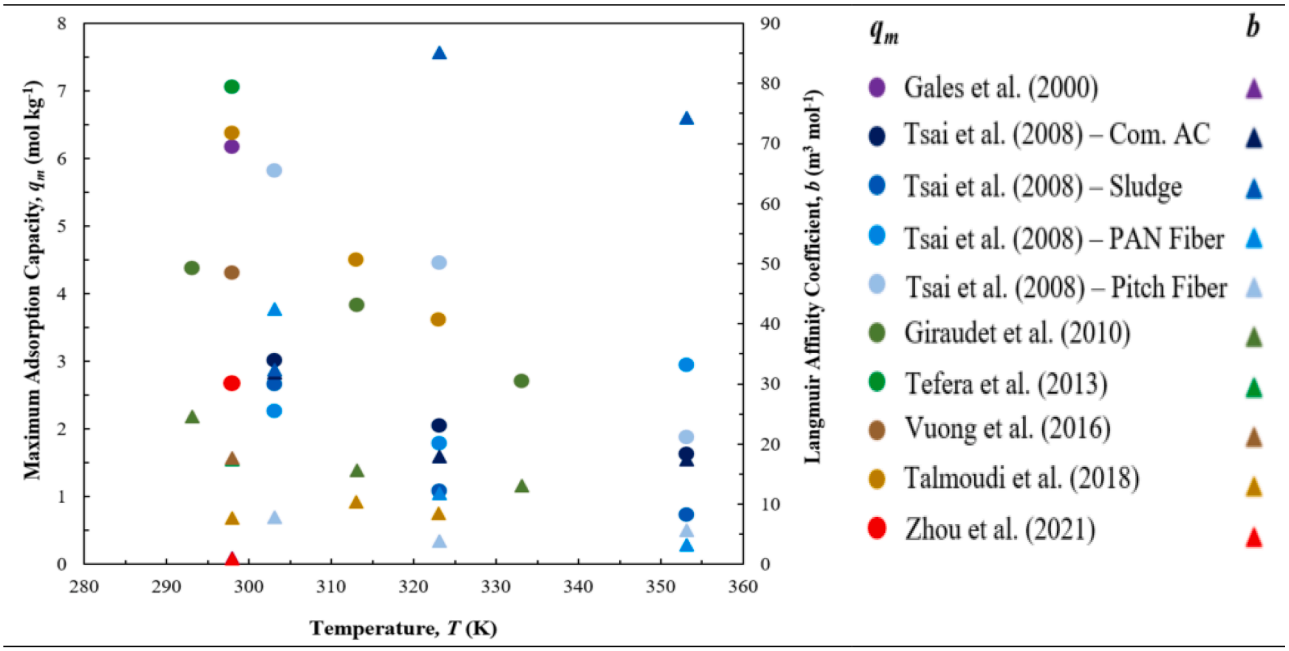

(a)

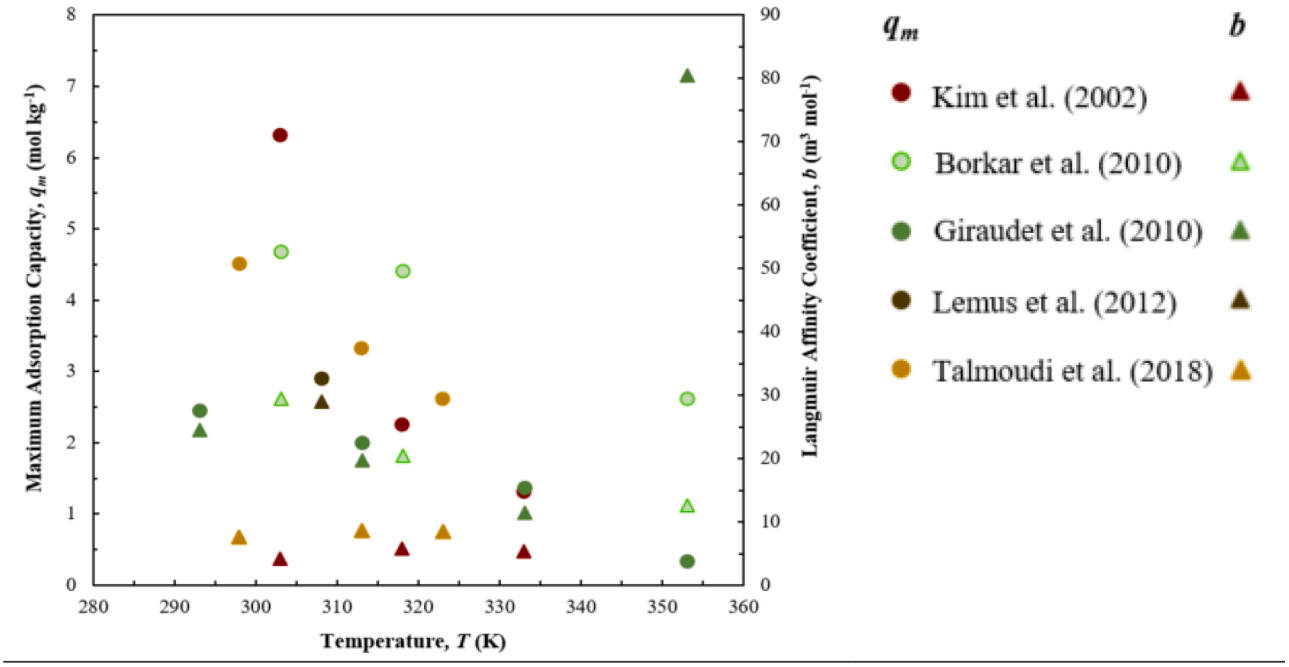

(b)

Fig. 2. Langmuir Isotherm parameter estimation for acetone (ACT) (a) and dichloromethane (DCM) (b).

phase concentration at equilibrium with $C_{0,i}$ and d_p the particle diameter.

The particle density is given by (Tefera et al., 2013, 2014):

$$\rho_p = \frac{\rho_b}{1-\varepsilon_b} \tag{7}$$

where ρ_b is the bed density and ε_b the bed porosity.

The bed porosity is given by (Tefera et al., 2013, 2014):

$$\varepsilon_b = 0.379 + \frac{0.078}{\left(\frac{D}{d_p}\right) - 1.8} \tag{8}$$

where D is the column internal diameter and d_p is the particle diameter.

The particle porosity is given by (Tefera et al., 2013, 2014):

$$\varepsilon_p = V_{pore}\rho_p \tag{9}$$

where V_{pore} is the adsorbent pore volume.

The particle tortuosity is given by (Tefera et al., 2013, 2014):

$$\tau_p = \frac{1}{\varepsilon_p^2} \tag{10}$$

where ε_p is the particle porosity.

The adsorbed phase concentration at equilibrium with $C_{0,i}$ is given by

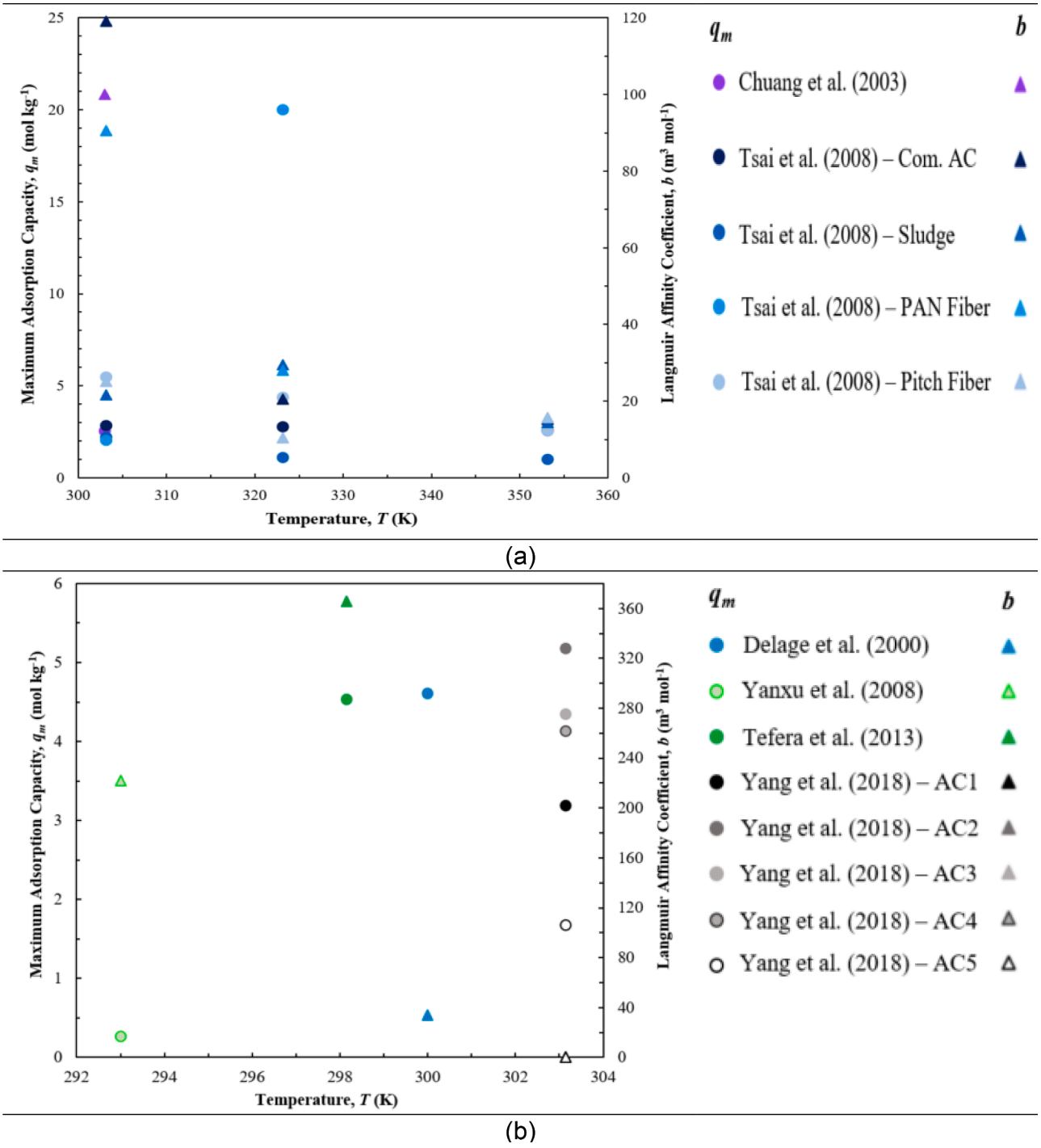

Fig. 3. Langmuir Isotherm parameter Estimation for chloroform (TCM) (a) and toluene (TOL) (b).

(Tefera et al., 2013, 2014):

$$C_{s0,i} = \rho_b q_{e,i} \tag{11}$$

where ρ_b is the bed porosity and $q_{e,i}$ is the inlet PT adsorbent equilibrium capacity.

The Knudsen diffusivity is given by (Ruthven, 1984):

$$D_{k,i} = 97 r_p \sqrt{\frac{T}{M_{rA}}} \tag{12}$$

where $D_{k,i}$ is the Knudsen diffusivity, r_p is the average pore radius, while T and M_{rA} are the temperature and VOC molecular weight.

The effective diffusivity is given by (Tefera et al., 2013, 2014):

$$\frac{1}{D_{eff,i}} = \frac{1}{D_{AB,i}} + \frac{1}{D_{k,i}} \tag{13}$$

The Bosanquet formula of Eq. (13), thus Eq. (6), is verified (Krishna and van Baten, 2012) for the estimation of the effective diffusivity ($D_{eff,i}$).

Adsorption equilibrium is assumed to obey the Extended Langmuir Model, described as follows:

$$q_{e,i} = \frac{q_{m,i} b_i C_i}{1 + \sum b_i C_i} \tag{14}$$

$$b_i = b_{o,i} exp\left(\frac{-\Delta H_{ad,i}}{RT}\right) \tag{15}$$

where $q_{e,i}$ is the equilibrium adsorption capacity of i, $q_{m,i}$ is the maximum adsorption capacity of i, b_i the Langmuir affinity coefficient, $b_{o,i}$ is the pre-exponential Langmuir affinity coefficient constant and $\Delta H_{ad,i}$ is the heat of adsorption.

The energy balance for the fluid and solid phases as well as the parameter main equations based on Ruthven (1984), Suzuki (1990) and Knox et al. (2016) are as follows:

$$\left(\rho_g C_{pg} + \frac{(1-\varepsilon_b)}{\varepsilon_b}\rho_p C_{pp}\right)\frac{\partial T}{\partial t} = k_{ez}\frac{\partial^2 T}{\partial z^2} - \rho_g C_{pg}\frac{\partial (uT)}{\partial z} + \frac{(1-\varepsilon_b)}{\varepsilon_b}\sum_{i=1}^{n}\Delta H_{ad,i}\frac{\partial q_i}{\partial t} - \frac{2h_o}{\varepsilon_b R_p}(T - T_w) \tag{16}$$

where T_w is the wall temperature, ρ_g is the gas density, Cp_g is the specific heat capacity of the gas, Cp_p is the specific heat capacity of the particle, k_{ez} is the effective axial thermal conductivity, R_p is the particle radius, T is the temperature and h_o is the overall heat transfer coefficient.

The effective thermal conductivity is given by (Knox et al., 2016):

$$k_{eff} = k_g\left(\frac{k_p}{k_g}\right)^n \tag{17}$$

$$n = 0.28 - 0.757\log_{10}\varepsilon_b - 0.057\log_{10}\left(\frac{k_p}{k_g}\right) \tag{18}$$

where k_{eff} is the effective thermal conductivity, k_g is the gas thermal conductivity, k_p is the particle thermal conductivity and n is the Krupickza equation parameter.

The effective axial thermal conductivity is given by (Knox et al., 2016):

$$k_{ez} = k_g\left(\frac{k_{eff}}{k_g} + 0.75PrRe\right) \tag{19}$$

The overall heat transfer coefficient is given by (Ruthven, 1984):

$$\frac{1}{h_o d} = \frac{1}{dh_{int}} + \frac{x}{k_w d_{lm}} \tag{20}$$

where h_{int} is the internal heat transfer coefficient, k_w is the wall thermal conductivity, x is the wall thickness and d_{lm} is the mean logarithmic column diameter.

The internal heat transfer coefficient is given by (Ruthven, 1984):

$$h_{int} = \frac{k_g}{2R}\left[2.03Re^{0.8}\exp\left(-6\frac{R_p}{R}\right)\right] \tag{21}$$

where R is the internal column radius.

The pressure drop along the column is calculated using Ergun's equation (Ruthven, 1984; Suzuki, 1990):

$$-\frac{\partial P}{\partial z} = 150u\mu\frac{(1-\varepsilon_b)^2}{\varepsilon_b^2 d_p^2} + 1.75\rho_g u^2\frac{(1-\varepsilon_b)}{\varepsilon_b d_p} \tag{22}$$

where μ is gas viscosity and P is pressure.

The system boundary conditions at the column inlet ($z = 0$) can be written as follows:

$$D_{z,i}\frac{\partial C_i(z=0,t)}{\partial z} = -u\left(C_{o,i} - C_i\right) \tag{23}$$

$$k_{z,i}\frac{\partial T(z=0,t)}{\partial z} = -uC_{pg}\rho_g(T_{in} - T) \tag{24}$$

$$u(0) = \frac{V_s}{\varepsilon_b} \tag{25}$$

The boundary conditions at the column outlet ($z = L$) are:

$$\frac{\partial C_i(z=L,t)}{\partial z} = 0 \tag{26}$$

$$\frac{\partial T(z=L,t)}{\partial z} = 0 \tag{27}$$

$$\frac{\partial u(L)}{\partial z} = 0 \tag{28}$$

The initial conditions at $t = 0$ for $0 \le z \le L$:

$$C_i(z, t=0) = 0 \tag{29}$$

$$q_i(z, t=0) = 0 \tag{30}$$

$$T = (z,\ t=0) = T_{in} \tag{31}$$

Moment analysis (Ruthven, 1984), and more specifically the analysis of the first moment, allows the prediction of the mean residence time of adsorbates in a given adsorption column based on the flowrate, thermodynamics of the system and flowrate, thus completely not dependant on kinetics:

$$\mu_{RT,i} = \frac{L}{u}\left[1 + \frac{(1-\varepsilon)}{\varepsilon}H_i\right] \tag{32}$$

where $\mu_{RT,i}$ is the mean residence time of component i, L is the column length, and H_i is the dimensionless Henry's constant of component i.

In this work, the dimensionless Henry's constant is calculated by:

$$H_i = \rho_p q_{m,i} b_i \tag{33}$$

With a formula similar to the mean residence time, the time required for a travelling shock to reach the column outlet can also be predicted (Ruthven, 1984; Kotchine, 1926):

$$t_{shock,i} = \frac{L}{u}\left(1 + \frac{(1-\varepsilon)}{\varepsilon}\frac{q_{\rho e,i}}{C_i}\right) \tag{34}$$

$$q_{\rho e,i} = \rho_p\frac{q_{m,i} b_i C_i}{1 + b_i C_i} \tag{35}$$

where $t_{shock,i}$ is the shock breakthrough time of component i and $q_{\rho e,i}$ is the equilibrium concentration of component i in mol m^{-3}.

The relative errors between the mean residence time (Eq. 32) and the $t_{95\%}$ of Fig. 5 plots are computed as follows:

$$\%RE = \frac{100\left(t_{95\%} - \mu_{RT,i}\right)}{t_{95\%}} \tag{36}$$

The relative errors between the shock breakthrough time (Eq. (34)) and the $t_{95\%}$ of Fig. 5 plots are computed as follows:

$$\%RE = \frac{100\left(t_{95\%} - t_{shock,i}\right)}{t_{95\%}} \tag{37}$$

3.1. Main model parameters & case studies

The developed model was employed to examine the adsorption of DCM-acetone according to the conditions set out by Talmoudi et al. (2018) (Table 3 CS0) using nitrogen as the carrier gas on an activated carbon bed, with the exception of the Langmuir Isotherm parameters; our model uses our own estimated Langmuir Isotherm parameter values for DCM and Tefera et al. (2013) for acetone for greater reliability. Then, our model was used to perform a temperature sensitivity analysis on the DCM-Acetone mixture of CS0 to examine the effect of different operating temperatures on breakthrough behaviour.

Table 3
Temperature sensitivity analysis: Main operational parameters for the DCM-ACT binary mixture.

System	$\Delta H_{ad,i}$ ($J\ mol^{-1}$)	$D_{z,i}$ ($m^2\ s^{-1}$)	T_{in} (K)	L (m)	C (ppm_v)	V_s ($m\ s^{-1}$)	q_m ($mol\ kg^{-1}$)	ε_b	k_{LDF} (s^{-1})	b_o ($m^3\ mol^{-1}$)	*Fig.*
DCM-ACT (CS0)	40,000	0.0008	298	0.100	2000	0.170	4.51	0.39	$1.39{\cdot}10^{-4}$	$7.41{\cdot}10^{-7}$	4a
	51,100	0.0008			500		7.06		$3.05{\cdot}10^{-5}$	$1.96{\cdot}10^{-8}$	
DCM-ACT	40,000	0.0008	298	0.100	2000	0.170	4.51	0.39	$1.39{\cdot}10^{-4}$	$7.41{\cdot}10^{-7}$	4b
	51,100	0.0008			500		7.06		$3.05{\cdot}10^{-5}$	$1.96{\cdot}10^{-8}$	
DCM-ACT	40,000	0.0008	293	0.100	2000	0.170	4.51	0.39	$1.14{\cdot}10^{-4}$	$7.41{\cdot}10^{-7}$	4b
	51,100	0.0008			500		7.06		$3.48{\cdot}10^{-5}$	$1.96{\cdot}10^{-8}$	
DCM-ACT	40,000	0.0008	288	0.100	2000	0.170	4.51	0.39	$1.04{\cdot}10^{-4}$	$7.41{\cdot}10^{-7}$	4b
	51,100	0.0008			500		7.06		$2.94{\cdot}10^{-5}$	$1.96{\cdot}10^{-8}$	

Table 4
Temperature sensitivity analysis: Main thermophysical properties for the DCM-ACT binary mixture.

System	ρ_b (kg m^{-3})	D (m)	T_{in} (K)	ε_p	d_p (m)	C_{pp} (J kg^{-1} K^{-1})	C_{pg} (J kg^{-1} K^{-1})	k_{ez} (W m^{-1} K^{-1})	h_o (W m^{-2} K^{-1})	h_{int} (W m^{-2} K^{-1})	k_w (W m^{-1} K^{-1})	*x (m)*	*Fig.*
DCM-ACT (CS0)	250	0.01	298	0.36	0.001	706.7	1039	0.21	4.55	4.56	14.2	0.001	4a
DCM-ACT	250	0.01	298	0.36	0.001	706.7	1039	0.21	4.55	4.56	14.2	0.001	4b
DCM-ACT	250	0.01	293	0.36	0.001	706.7	1039	0.22	4.52	4.53	14.2	0.001	4b
DCM-ACT	250	0.01	288	0.36	0.001	706.7	1039	0.22	4.51	4.52	14.2	0.001	4b

The set of PDEs is solved using second order orthogonal collocation on finite elements with 30 discretisation points in the gPROMS Process 2.0.0 software suite. For all cases considered, the DASolver DAEBDF is employed, which uses a variable time step and variable order Backward Finite Differentiation Formulae. Moreover, the DOSolver is CVP_SS, the EDSolver is EXPDES and the PESolver is MAXLKHD. The viscosities are computed from Wilke's equation, while densities are determined through pure component data via mixing rules (NIST, 2021). The main system parameters are in Table 3.

Table 4 summarizes the main structural (column and adsorbent) and thermal parameter values of the systems:

Next, the model has been used to explore the adsorption of binary mixtures of pharmaceutically relevant VOCs (acetone, dichloromethane, chloroform and toluene) on an activated carbon fixed-bed column using air as the carrier gas (CS1-CS15) for two different temperatures (T = 293 K, T = 300 K) and two different bed porosities ($\varepsilon_b = 0.35$, $\varepsilon_b = 0.38$). Air is assumed a binary mixture (N_2:O_2 = 79:21% v/v) and Langmuir Isotherm parameters ($q_{m,i}$ and b_i) are taken from Tefera et al. (2013) for acetone, from Chuang et al. (2003) for chloroform, and from Delage et al. (2000) for toluene, respectively. Langmuir Isotherm parameters for dichloromethane ($q_{m,i}$ and b_i) are estimated from data by Talmoudi et al. (2018). Heats of adsorption are used as per in these four papers. The main structural (column, adsorbent) and thermal parameter values are given in Table 5.

Table 5
Thermophysical property values for binary mixture case study (CS) simulations.

System	ρ_b (kg m^{-3})	D (m)	T_{in} (K)	ε_p	d_p (m)	C_{pp} (J kg^{-1} K^{-1})	C_{pg} (J kg^{-1} K^{-1})	k_{ez} (W m^{-1} K^{-1})	h_o (W m^{-2} K^{-1})	h_{int} (W m^{-2} K^{-1})	k_w (W m^{-1} K^{-1})	*x (m)*	*Fig.*
DCM-ACT (CS1)	606	0.0152	300	0.56	0.00075	706.7	1013	0.67	52.90				
										53.08	14.2	0.001	5a
DCM-ACT (CS2)	606	0.0152	293	0.56	0.00075	706.7	1013	0.69	53.70				
										53.89	14.2	0.001	
DCM-ACT (CS3)	606	0.0152	300	0.53	0.00075	706.7	1013	0.67	52.90				
										53.08	14.2	0.001	5b
DCM-ACT (CS4)	606	0.0152	293	0.53	0.00075	706.7	1013	0.69	53.70				
										53.89	14.2	0.001	
DCM-TCM (CS5)	606	0.0152	300	0.56	0.00075	706.7	1012	0.67	53.16				
										53.35	14.2	0.001	5c
DCM-TCM (CS6)	606	0.0152	293	0.56	0.00075	706.7	1012	0.69	53.63				
										53.82	14.2	0.001	
DCM-TCM (CS7)	606	0.0152	300	0.53	0.00075	706.7	1012	0.67	53.16				
										53.35	14.2	0.001	5d
DCM-TCM (CS8)	606	0.0152	293	0.53	0.00075	706.7	1012	0.69	53.63				
										53.82	14.2	0.001	
DCM-TOL (CS9)	606	0.0152	300	0.56	0.00075	706.7	1013	0.67	37.17				
										37.26	14.2	0.001	5e
DCM-TOL (CS10)	606	0.0152	293	0.56	0.00075	706.7	1013	0.68	53.62				
										53.81	14.2	0.001	
DCM-TOL (CS11)	606	0.0152	300	0.53	0.00075	706.7	1013	0.67	40.59				
										40.70	14.2	0.001	5f
DCM-TOL (CS12)	606	0.0152	293	0.53	0.00075	706.7	1013	0.68	53.62				
										53.81	14.2	0.001	
TCM-ACT (CS13)	606	0.0152	300	0.56	0.00075	706.7	1013	0.67	37.21				
										37.30	14.2	0.001	6a
TCM-TOL (CS14)	606	0.0152	300	0.56	0.00075	706.7	1013	0.67	39.83				
										39.93	14.2	0.001	6b
TOL-ACT (CS15)	606	0.0152	300	0.56	0.00075	706.7	1014	0.67	39.78				
										39.88	14.2	0.001	6c

Table 6
Binary mixture Case Studies (CS) and main parameters for adsorption dynamic simulations.

System	$D_{z,i}$ (m^2 s^{-1})	$\Delta H_{ad,i}$ (J mol^{-1})	T_{in} (K)	L (m)	x_{VOC}	V_s (m s^{-1})	q_m (mol kg^{-1})	ε_b	k_{LDF} (s^{-1})	b_0 (m^3 mol^{-1})	Fig.
DCM-ACT (CS1)	0.00238	40,000	300	0.065	250	0.914	4.51	0.38	$2.16{\cdot}10^{-4}$	$7.41{\cdot}10^{-7}$	5a
	0.00238	51,100			250		7.06		$8.16{\cdot}10^{-5}$	$1.96{\cdot}10^{-8}$	
DCM-ACT (CS2)	0.00235	40,000	293	0.065	250	0.914	4.51	0.38	$2.34{\cdot}10^{-4}$	$7.41{\cdot}10^{-7}$	
	0.00236	51,100			250		7.06		$5.46{\cdot}10^{-5}$	$1.96{\cdot}10^{-8}$	
DCM-ACT (CS3)	0.00258	40,000	300	0.065	250	0.914	4.51	0.35	$1.87{\cdot}10^{-4}$	$7.41{\cdot}10^{-7}$	5b
	0.00259	51,100			250		7.06		$7.08{\cdot}10^{-5}$	$1.96{\cdot}10^{-8}$	
DCM-ACT (CS4)	0.00255	40,000	293	0.065	250	0.914	4.51	0.35	$1.99{\cdot}10^{-4}$	$7.41{\cdot}10^{-7}$	
	0.00256	51,100			250		7.06		$4.63{\cdot}10^{-5}$	$1.96{\cdot}10^{-8}$	
DCM-TCM (CS5)	0.00148	40,000	300	0.065	250	0.914	4.51	0.38	$4.31{\cdot}10^{-4}$	$7.41{\cdot}10^{-7}$	5c
	0.00140	44,769			250		2.49		$3.85{\cdot}10^{-5}$	$1.91{\cdot}10^{-6}$	
DCM-TCM (CS6)	0.00236	40,000	293	0.065	250	0.914	4.51	0.38	$3.92{\cdot}10^{-4}$	$7.41{\cdot}10^{-7}$	
	0.00229	44,769			250		2.49		$3.22{\cdot}10^{-5}$	$1.91{\cdot}10^{-6}$	
DCM-TCM (CS7)	0.00258	40,000	300	0.065	250	0.914	4.51	0.35	$3.65{\cdot}10^{-4}$	$7.41{\cdot}10^{-7}$	5d
	0.00250	44,769			250		2.49		$3.29{\cdot}10^{-5}$	$1.91{\cdot}10^{-6}$	
DCM-TCM (CS8)	0.00256	40,000	293	0.065	250	0.914	4.51	0.35	$3.32{\cdot}10^{-4}$	$7.41{\cdot}10^{-7}$	
	0.00248	44,769			250		2.49		$2.73{\cdot}10^{-5}$	$1.91{\cdot}10^{-6}$	
DCM-TOL (CS9)	0.00148	40,000	300	0.065	250	0.914	4.51	0.38	$2.76{\cdot}10^{-4}$	$7.41{\cdot}10^{-7}$	5e
	0.00134	45,500			250		4.61		$5.33{\cdot}10^{-5}$	$4.06{\cdot}10^{-7}$	
DCM-TOL (CS10)	0.00235	40,000	293	0.065	250	0.914	4.51	0.38	$2.21{\cdot}10^{-4}$	$7.41{\cdot}10^{-7}$	
	0.00223	45,500			250		4.61		$3.94{\cdot}10^{-5}$	$4.06{\cdot}10^{-7}$	
DCM-TOL (CS11)	0.00258	40,000	300	0.065	250	0.914	4.51	0.35	$2.39{\cdot}10^{-4}$	$7.41{\cdot}10^{-7}$	5f
	0.00243	45,500			250		4.61		$4.48{\cdot}10^{-5}$	$4.06{\cdot}10^{-7}$	
DCM-TOL (CS12)	0.00255	40,000	293	0.065	250	0.914	4.51	0.35	$1.87{\cdot}10^{-4}$	$7.41{\cdot}10^{-7}$	
	0.00242	45,500			250		4.61		$3.34{\cdot}10^{-5}$	$4.06{\cdot}10^{-7}$	
TCM-ACT (CS13)	0.00140	44,769	300	0.065	250	0.914	2.49	0.38	$4.10{\cdot}10^{-5}$	$1.91{\cdot}10^{-6}$	6a
	0.00148	51,100			250		7.06		$1.59{\cdot}10^{-4}$	$1.96{\cdot}10^{-8}$	
TCM-TOL (CS14)	0.00140	44,769	300	0.065	250	0.914	2.49	0.38	$4.42{\cdot}10^{-5}$	$1.91{\cdot}10^{-6}$	6b
	0.00134	45,500			250		4.61		$9.50{\cdot}10^{-5}$	$4.06{\cdot}10^{-7}$	
TOL-ACT (CS15)	0.00134	45,500	300	0.065	250	0.914	4.61	0.38	$5.58{\cdot}10^{-5}$	$4.06{\cdot}10^{-7}$	6c
	0.00148	51,100			250		7.06		$1.01{\cdot}10^{-4}$	$1.96{\cdot}10^{-8}$	

The main parameters used in Case Studies (CS) simulations for the binary mixtures are in Table 6.

3.2. Dynamic simulation (gPROMS) results

The developed model has been first validated against the published experimental data of Talmoudi et al. (2018) for the adsorption of binary DCM-acetone using N_2 as the carrier gas (Table 3, CS0) and then used to simulate the adsorption of binary mixtures of pharmaceutically relevant VOCs (acetone, dichloromethane, chloroform and toluene) on an activated carbon fixed-bed column using air as the carrier gas (Table 6, CS1-CS15). The binary mixtures of dichloromethane with chloroform, dichloromethane with toluene and dichloromethane with acetone are simulated in adsorption scenarios of two different temperatures and two different bed porosities each (CS1-CS3, CS7-CS15). Breakthrough curves, showing the component concentration at column outlet, of the

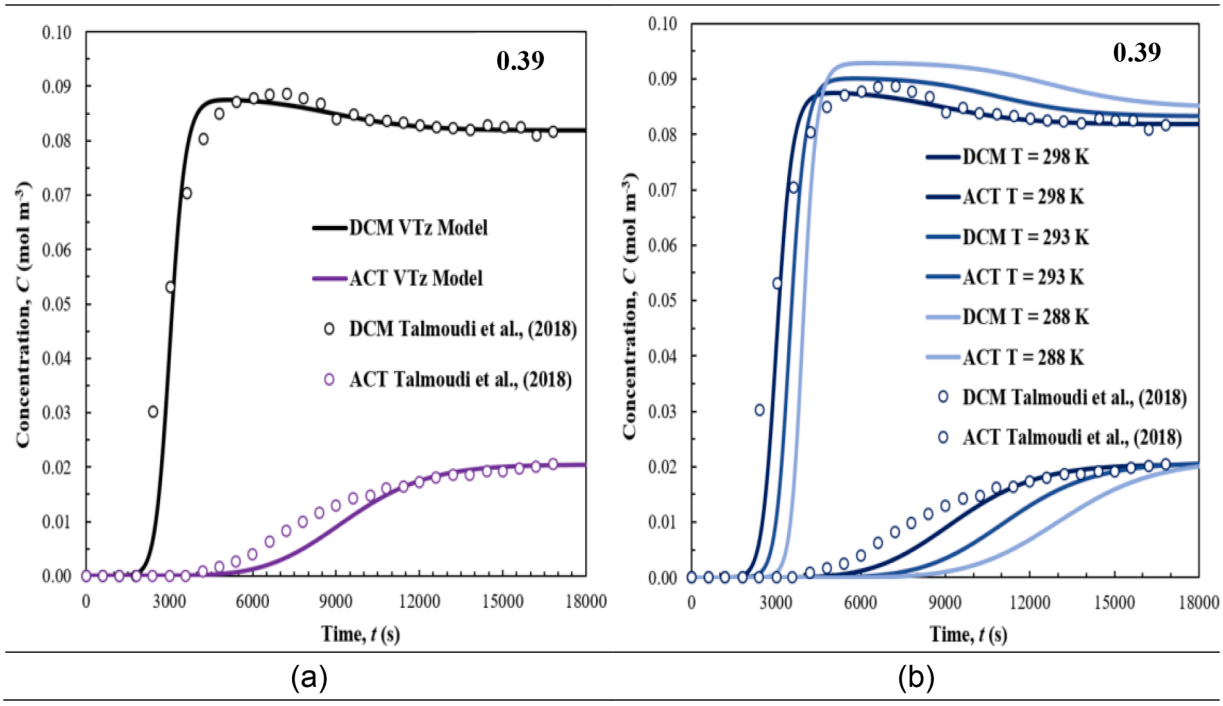

Fig. 4. Model validation (a) and temperature sensitivity analysis (b) for the DCM-ACT binary mixture system (bed outlet).

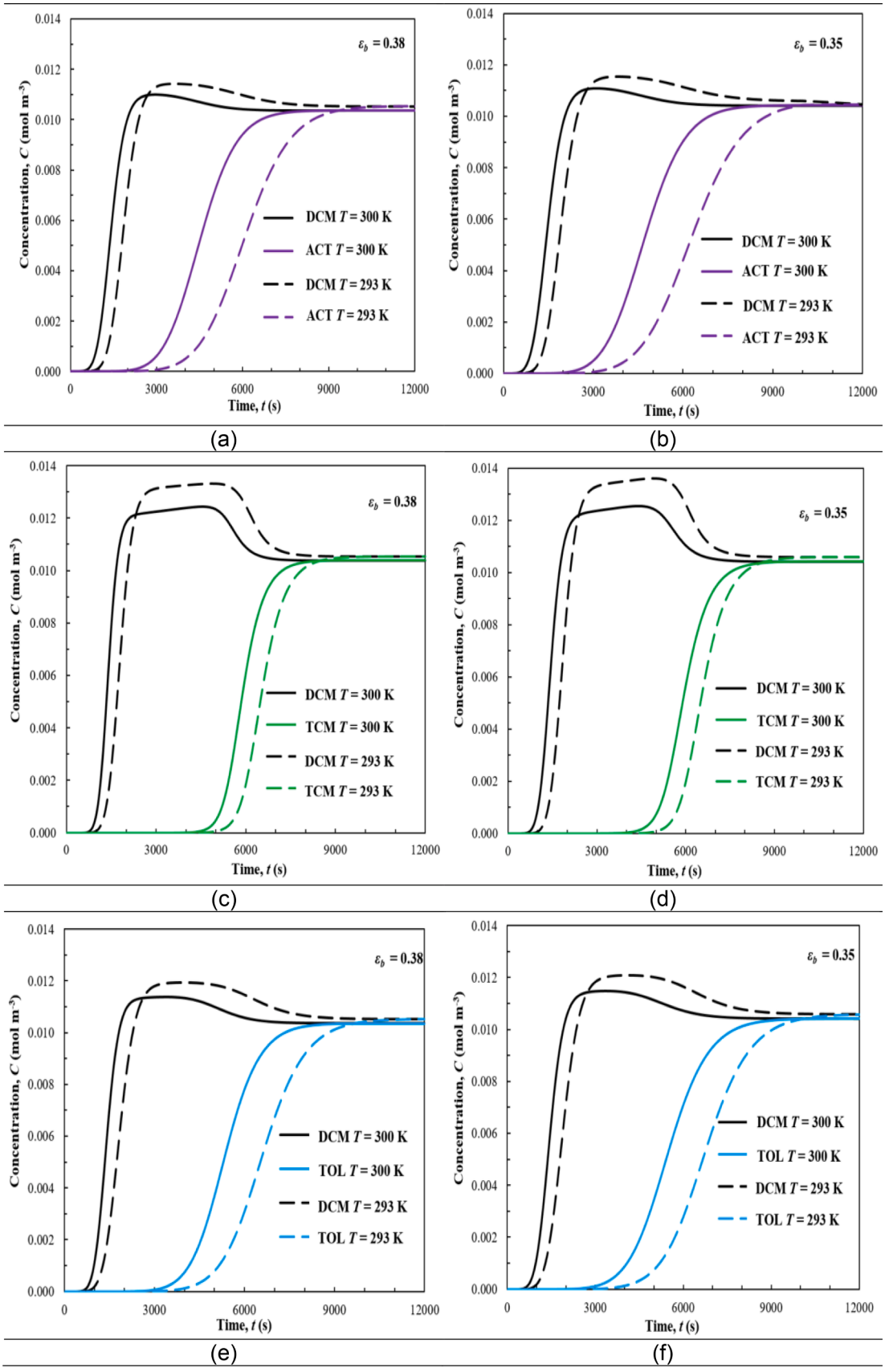

Fig. 5. Binary system breakthrough comparison at T = 293, 300 K and for ε_b = 0.35, 0.38 (bed outlet).

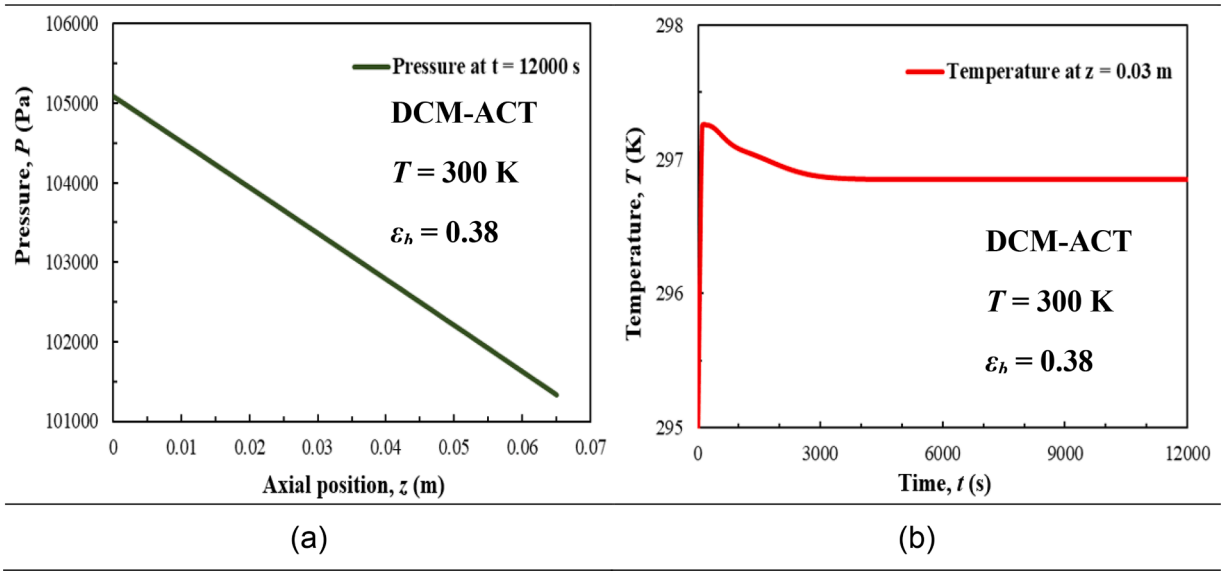

Fig. 6. Pressure at t = 12,000 s and temperature at z = 0.03 m for the DCM-ACT binary mixture (CS1).

Table 7
Key time metrics from dichloromethane-acetone (DCM-ACT) CS runs.

	DCM-ACT								
	T (K)	ε_b	t_{shock} (s) Eq. (34)	μ_{RT} (s) Eq. (32)	$t_{5\%}$ (s) Fig. 5a, b	$t_{95\%}$ (s) Fig. 5a, b	t_{drt} (s) Fig. 5a, b	%R.E. t_{shock}	%R.E. μ_{RT}
DCM	293	0.35	1760	1950	1206	8607	7401	79.55	77.34
ACT			6115	7690	4112	8607	4495	28.95	10.65
DCM	293	0.38	1756	1945	1183	8283	7100	78.80	76.52
ACT			6103	7671	4026	8283	4257	26.32	7.39
DCM	300	0.35	1245	1329	825	6455	5630	80.71	79.41
ACT			4063	4714	3018	6455	3437	37.06	26.97
DCM	300	0.38	1242	1326	810	6195	5385	79.95	78.60
ACT			4052	4702	2916	6195	3279	34.59	24.10

examined binary mixture systems are presented in Figs. 4–6, while key breakthrough time metrics have been summarised in Tables 7–10.

Our model is successfully validated (Fig. 4a) against published experimental breakthrough curves which dictated model inputs (Talmoudi et al., 2018), using our own estimated Langmuir Isotherm parameters. The DCM breakthrough curve has been captured with higher accuracy compared to the one published by Talmoudi et al. (2018) plot for their experimental data, while a slight mismatch is observed after breakthrough for acetone at the curve slope. The discrepancy (present in both efforts) can be attributed to one-dimensional model limitations.

The same dichloromethane-acetone mixture as the base case (CS0) is employed for a temperature sensitivity analysis in Fig. 4b, as the temperature is one of the key parameters affecting adsorption behaviour. Three different temperatures have been investigated and in all cases, DCM exits the column outlet at a higher concentration compared to its inlet. Results indicate that with rising temperature, the maximum concentration of DCM recorded at the column outlet, declines. Moreover, as expected by adsorption theory, with rising temperature the breakthrough onset time for both VOCs becomes shorter, due to adsorption exothermicity.

The mixture of dichloromethane with acetone has also been used in case studies for two different temperatures and two different bed porosities, and the relevant plots are presented in Fig. 5a and 5b. In all scenarios considered, DCM emerges at the column outlet in a concentration higher than its inlet concentration. Breakthrough onset is here defined as the time when $C_{outlet,i} = 5\%C_{feed,i}$, while breakthrough duration is defined here as the time from $5\%C_{feed}$ to $95\%C_{feed}$ observed at the column outlet.

Higher temperature results in earlier breakthrough onset and shorter breakthrough duration. In Fig. 5a, where $\varepsilon_b = 0.38$, breakthrough onset at 293 K is 46.05% later for DCM and 38.07% later for acetone compared to 300 K. Breakthrough duration at $\varepsilon_b = 0.38$ for DCM is 36.38% longer at 293 K than at 300 K, whereas acetone's at 293 K is 37.10% longer than at 300 K. In Fig. 5b, where $\varepsilon_b = 0.35$, the breakthrough onset time of DCM is 46.89% later at 293 K than 300 K, and 36.70% later for acetone. Regarding breakthrough duration at $\varepsilon_b = 0.35$, DCM's is 34.74% longer at 293 K compared to 300 K, while acetone's is 35.71% longer at 293 K compared to 300 K.

Bulk bed porosity also affects breakthrough times. At $T = 293$ K and $\varepsilon_b = 0.35$ (Fig. 5b), DCM and acetone reach breakthrough at $t = 1206$s and $t = 4112$ s respectively, values which are 1.94% and 2.14% larger compared to the breakthrough onset times at bed porosity $\varepsilon_b = 0.38$ (Fig. 5a). At 300 K and $\varepsilon_b = 0.35$ (Fig. 5b), the same trend is observed, with DCM's breakthrough onset being 1.36% later compared to 0.38, and acetone's 3.16% compared to 0.38 (Fig. 5a). Breakthrough duration for DCM is 2.12% larger and for acetone 2.07% larger at 293 K and $\varepsilon_b = 0.35$ compared to 0.38. At 300 K and $\varepsilon_b = 0.35$, the trend persists, with DCM's breakthrough duration 3.36% longer and acetone's 3.11% longer compared to 0.38.

The mixture of dichloromethane with chloroform (TCM) was also employed for case studies at two different temperatures and two different bed porosities which can be seen in Fig. 5c and 5d. In all scenarios considered, the order of affinity persists with DCM being weakly adsorbed. For the same ε_b (Fig. 5c) breakthrough onset at 293 K is 71.20% later for DCM and 2.16% earlier for TCM compared to 300 K. In Fig. 5d, the breakthrough onset time of DCM is 35.96% later at 293 K than at 300 K, and 13.67% later for TCM. In Fig. 5c, the breakthrough duration of DCM is 15.60% longer at 293 K than at 300 K, whereas

Table 8
Key time metrics from dichloromethane-toluene (DCM-TOL) CS runs.

	DCM-TOL								
	T (K)	ε_b	t_{shock} (s) Eq. (34)	μ_{RT} (s) Eq. (32)	$t_{5\%}$ (s) Fig. 5c, d	$t_{95\%}$ (s) Fig. 5c, d	t_{drt} (s) Fig. 5c, d	%R.E. t_{shock}	%R.E. μ_{RT}
DCM	293	0.35	1765	1950	1168	8881	7713	80.13	78.04
TOL			6757	10,441	4766	8881	4115	23.92	−17.57
DCM	293	0.38	1761	1945	1150	8637	7487	79.61	77.48
TOL			6736	10,414	4745	8637	3892	22.01	−20.57
DCM	300	0.35	1242	1329	858	7333	6475	83.06	81.88
TOL			5023	6752	3694	7333	3639	31.50	7.92
DCM	300	0.38	1239	1326	885	6950	6065	82.17	80.92
TOL			5008	6735	3818	6950	3132	27.94	3.09

Table 9
Key time metrics from dichloromethane-chloroform (DCM-TCM) CS runs.

	DCM-TCM								
	T (K)	ε_b	t_{shock} (s) Eq. (34)	μ_{RT} (s) Eq. (32)	$t_{5\%}$ (s) Fig. 5e, f	$t_{95\%}$ (s) Fig. 5e, f	t_{drt} (s) Fig. 5e, f	%R.E. t_{shock}	%R.E. μ_{RT}
DCM	293	0.35	1751	1949	1240	7865	6625	77.74	75.22
TCM			6764	19,651	5537	7865	2328	14.00	−149.85
DCM	293	0.38	1746	1944	1379	7758	6379	77.49	74.94
TCM			6750	19,601	5592	7758	2166	12.99	−152.66
DCM	300	0.35	1232	1480	912	7115	6203	82.68	79.20
TCM			5788	14,442	4871	7115	2244	18.65	−102.98
DCM	300	0.38	1229	1477	948	6892	5944	82.17	78.57
TCM			5773	14,405	5008	6892	1884	16.24	−109.01

TCM's at 293 K is 75.87% longer than at 300 K. In Fig. 5d, DCM breakthrough duration is 9.96% longer at 293 K compared to 300 K, while TCM's is 11.98% longer at 293 K compared to 300 K.

The breakthrough behaviour of the binary mixture of DCM-TCM is also clearly affected by bulk bed porosity (Fig. 5c vs. 5d). At 293 K and $\varepsilon_b = 0.35$ (Fig. 5d), DCM and TCM reach breakthrough at $t = 1240$s and $t = 5537$ s respectively, values which are 23.60% sooner and 13.00% later compared to the VOCs breakthrough onset times at bed porosity 0.38 (Fig. 5c) and 293 K. At 300 K and $\varepsilon_b = 0.35$ (Fig. 5b), DCM's breakthrough onset is 3.80% earlier and TCM's 2.74% earlier compared to $\varepsilon_b = 0.38$ at the same temperature (Fig. 5c). Breakthrough duration at 293 K and $\varepsilon_b = 0.35$ is for DCM 0.01% shorter and for TCM 24.70% shorter compared to 0.38. At 300 K and $\varepsilon_b = 0.35$, the trend is reversed, with DCM's breakthrough duration being 5.12% longer and TCM's 18.26% longer compared to 0.38.

The mixture of dichloromethane with toluene has been similarly used in case studies for two different temperatures and two different bed porosities (Fig 5e and 5f). In all scenarios considered the order of affinity remains with DCM exiting the column in concentrations higher than its inlet's. In Fig. 5e, where $\varepsilon_b = 0.38$, breakthrough onset at 293 K is 36.13% later for DCM and 29.02% later for toluene compared to 300 K. Moreover, breakthrough duration of DCM is 31.10% longer at 293 K than at 300 K, whereas toluene's breakthrough duration at 293 K is 37.84% longer than at 300 K. In Fig. 5f, where $\varepsilon_b = 0.35$, the breakthrough onset time of DCM is 46.89% later at 293 K than at 300 K, and 36.70% later for acetone.

Regarding breakthrough duration, at $\varepsilon_b = 0.35$, DCM's is 24.56% longer at 293 K compared to 300 K, while toluene's is 23.02% longer at 293 K compared to 300 K.

Finally, breakthrough behaviour of the dichloromethane-toluene mixture shows slight differences with varying bulk bed porosity (Fig. 5e vs. 5f). At 293 K and $\varepsilon_b = 0.35$ (Fig. 5f), DCM and toluene reach breakthrough at $t = 1168$s and $t = 4766$ s respectively, values which are 1.57% and 0.44% larger compared to the VOCs breakthrough onset times at bed porosity $\varepsilon_b = 0.38$ (Fig. 5e) and 293 K. At 300 K and $\varepsilon_b = 0.35$ (Fig. 5f), the trend is reversed, with DCM's breakthrough onset being 3.05% earlier compared to 0.38, and toluene's 3.25% earlier compared to 0.38 at the same temperature (Fig. 5e). Breakthrough duration at 293 K and $\varepsilon_b = 0.35$ is for DCM 1.46% longer and for toluene 2.42% longer compared to 0.38. At 300 K and $\varepsilon_b = 0.35$, the trend persists, with DCM's breakthrough duration being 6.79% longer and toluene's 14.77% longer compared to 0.38.

Figs. 6–8 introduce the pressure drop profile at $t = 12{,}000$ s and the temperature profile at $z = 0.03$ m for the mixtures of DCM-ACT, DCM-TCM and DCM-TOL at $T_{in} = 300$ K and $\varepsilon_b = 0.38$

(CS1, CS5 and CS 9 Table 6). For all cases presented, pressure drop, which follows Ergun's equation, is linear. Regarding the temperature profiles at $z = 0.03$ m, it is obvious that the temperature sharply rises when the gas mixture arrives, and immediately starts to drop as we approach the column outlet given the fact that the gas stream has an

Table 10
Key time metrics from the TCM-ACT, TCM-TOL and TOL-ACT system runs.

	TCM-ACT								
	T (K)	ε_b	t_{shock} (s) Eq. (34)	μ_{RT} (s) Eq. (32)	$t_{5\%}$ (s) Fig. 6a	$t_{95\%}$ (s) Fig. 6a	t_{drt} (s) Fig. 6	%R.E. t_{shock}	%R.E. μ_{RT}
TCM	300	0.38	5798	12,767	4538	6830	2292	15.11	−86.93
ACT			4052	4702	3097	6830	3733	40.67	31.16
	TCM-TOL								
TCM	300	0.38	5786	12,792	4024	6553	2529	11.69	−95.21
TOL			5018	6749	3626	6553	2927	23.42	−2.99
	TOL-ACT								
TOL	300	0.38	5018	6749	3663	6541	2878	23.28	−3.18
ACT			4071	4711	3080	6541	3461	37.76	27.98

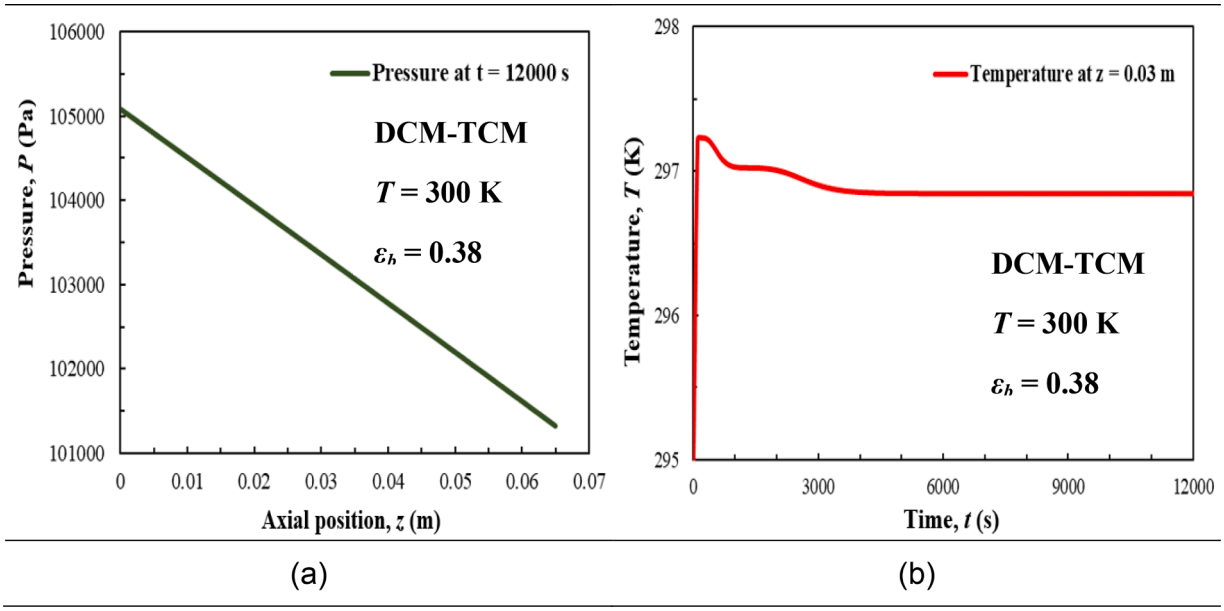

Fig. 7. Pressure at t = 12,000 s and temperature at z = 0.03 m for the DCM-TCM binary mixture (CS5).

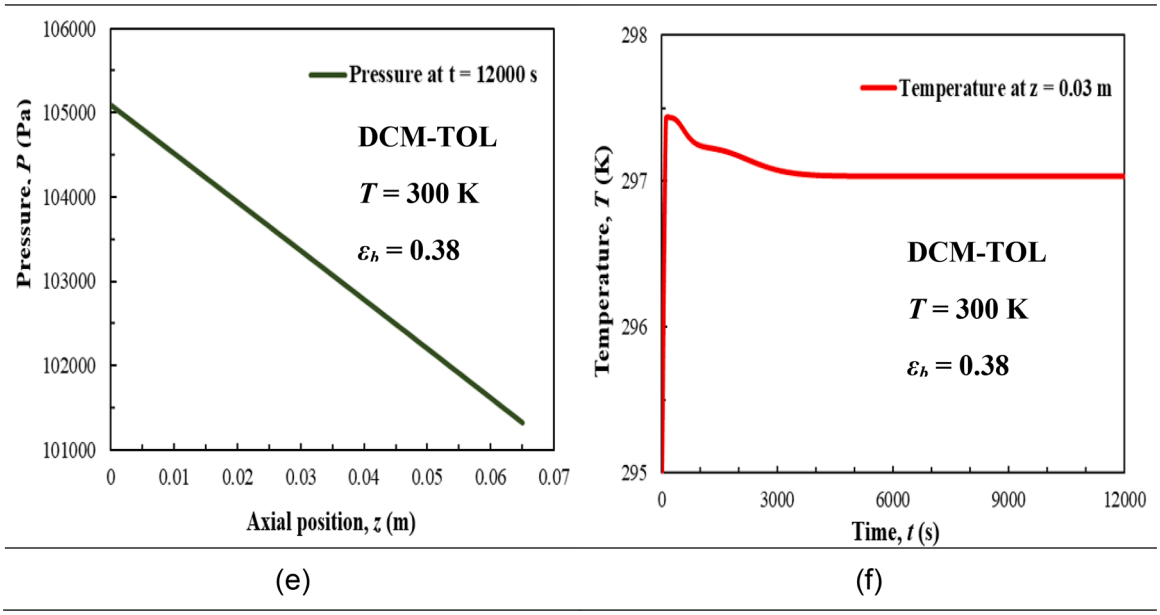

Fig. 8. Pressure at t = 12,000 s and temperature at z = 0.03 m for the DCM-TOL binary mixture (CS9).

inlet temperature of 300 K and the column walls 295 K. The plateaus observed at the beginning of the graph are a result of adsorption exothermicity and correspond to adsorption taking place at this axial position (z = 0.03 m).

Fig. 6a and 6b correspond to the DCM-ACT mixture (CS1). The pressure drop a t = 12,000 s is equal to 3755.6 Pa. In Fig. 6b, the maximum temperature reached is 297.26 K.

Fig. 7a shows the pressure drop of DCM-TCM (CS5), which is equal to 3755.52 Pa, while the maximum temperature observed in Fig. 7b is 297.23 K.

Lastly, the DCM-TOL (CS9) pressure and temperature profiles are presented in Fig. 8a and b. Pressure drop is 3758.40 Pa and T_{max} = 297.43 K.

The case studies of Figs. 6–8 show that the pressure drops are about 3.76 kPa under the examined conditions in laboratory scale columns while the temperature profiles show only but small temperature plateaus. These effects however would be magnified under industrial conditions and thus require careful flow adjustments to ensure process safety and operational expenditure minimisation.

The adsorption of the binary mixtures of chloroform with acetone (Fig. 9a), chloroform with toluene (Fig. 9b) and toluene with acetone (Fig. 9c) has also been investigated at 300 K and ε_b = 0.38. Amongst the three mixtures breakthrough characteristics, solvent-to-carbon affinity is correlated with molecular weight, with increasing molecular weight leading to higher affinity for the activated carbon. Therefore, chloroform (TCM) is the most strongly adsorbed mixture component, followed by toluene and then acetone. Chloroform (TCM), a solvent whose emissions are tightly regulated by the Scottish Environmental Protection Agency (SEPA), exits the column earlier when in a mixture with toluene, compared with one with acetone.

Harnessing simulation results to aid in production scheduling optimisation is essential to sustainable manufacturing (Akbar and Irohara,

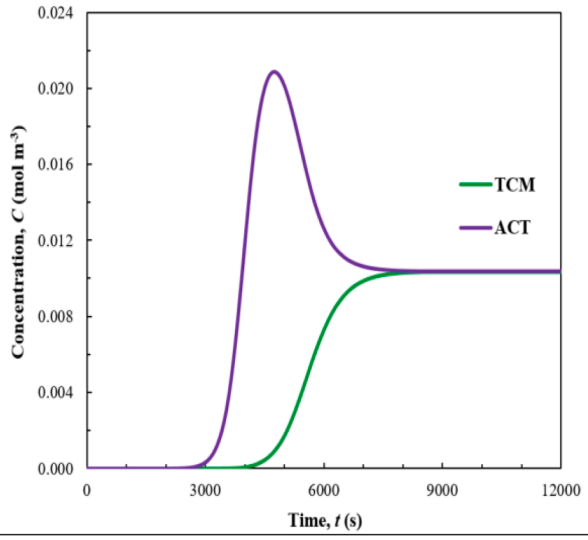

(a)

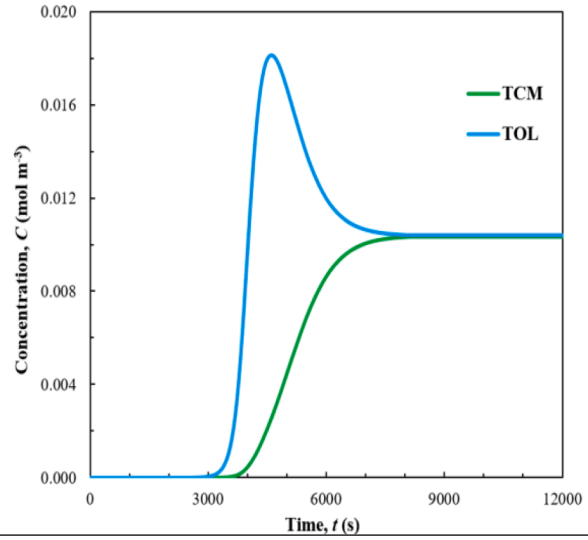

(b)

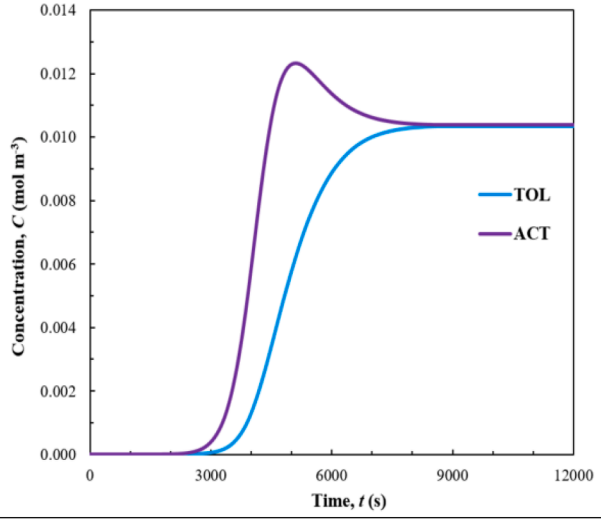

(c)

Fig. 9. Breakthrough concentration curves for three binary mixtures at $T = 300$ K and $\varepsilon_b = 0.38$ (bed outlet).

2018; Giret et al., 2015). Understanding VOC breakthrough patterns paves the way to emissions reduction and designing production scheduling paradigms not only in a way that satisfies demand, but also respecting the environment by minimising impact. The combination of solvents in a mixture, their quantities and the operational parameters could be the key to sustainably improving existing underperforming processes. This in turn translates into less waste-intensive end-of-pipe solutions for emissions control and unit operations that meet environmental and societal demands.

Table 7 presents key breakthrough metrics of the dichloromethane-acetone system in the cases investigated. Two theoretically derived predictive formulas Eqs. (32) and ((34)) can help us determine the shock breakthrough time (how long a single component's concentration front reaches the bed outlet) and the mean residence time (required for a single component to achieve breakthrough through a column). The breakthrough duration time, $t_{drt,i}$, is here defined as the time span between 5% breakthrough and 95% breakthrough, from dynamic simulations. Our simulation breakthrough completion times ($t_{95\%}$), from Fig. 5 plots, are used to define and compute relative errors compared with each of the two foregoing metrics Eq. (36) and ((37)). Results for DCM exhibit notable discrepancies from both theoretical time metrics of Eq. (32) and (34); closer agreement is achieved for acetone. The relative error for the mean residence time has a consistently smaller discrepancy compared to the shock breakthrough time error. These discrepancies are attributed to the fact that both theoretical metrics Eqs. (32) and ((34)) are derived for isothermal conditions and single-component Langmuir Isotherm adsorption, while our dynamic simulations concern the case of binary mixture (DCM-acetone) adsorption. However, theoretical predictive formulas clearly provide good order-of-magnitude estimates.

Table 8 presents the key breakthrough metrics for the dichloromethane-toluene system. Dynamic simulation breakthrough times (Fig. 5 c, d) are compared with mean residence and shock breakthrough time predictions (from Eqs. (32) and (34)). Errors computed for DCM indicate clear discrepancy from both theoretical metrics, but acceptable and quite reliable predictions are clearly achieved for both the mean residence and the shock breakthrough times. For toluene, the mean residence time shows consistently smaller discrepancies compared to the shock breakthrough time. Once again, all (small and larger) discrepancies can be safely attributed to the isothermal conditions and single-component Langmuir Isotherm adsorption used for Eqs. (32) and (24), but the latter can provide good first estimates for industrial operation.

Table 9 presents the same breakthrough metrics for the dichloromethane-chloroform system. Dynamic simulation results Fig. 5e, f) are again compared with mean residence and shock breakthrough time predictions (Eqs. (32) and ((34)) via relative error calculations Eqs. (36) and ((37)). Similarly to both previous binary system cases, we clearly observe that error metrics for DCM are considerably high (but within the same order of magnitude) for both theoretical metrics. Conversely, error metrics for chloroform display a more complicated landscape: the relative error for the shock breakthrough time is very promising and smaller than any other mixture (below 19% or better), implying the approximate predictive formula Eq. (34)) is quite suitable. Nevertheless, the mean residence time error is large - in fact larger than in both other systems. Also, relative errors are consistently negative, implying mean residence time overprediction. Once again, the discrepancies observed differ by metric as well as by component, and they can be attributed to the isothermal conditions and single-component Langmuir Isotherm adsorption which have been used in the literature for deriving Eqs. (32) and ((24). Nevertheless, these formulas can offer useful fast industrial predictions without/before dynamic simulations.

Table 10 introduces a set of key breakthrough metrics Eqs. (32) and ((34)) for the systems of chloroform (TCM) with acetone, chloroform with toluene and toluene with acetone for $T = 300$ K and bulk bed porosity of 0.38 in all cases. Shock breakthrough time and mean residence time relative errors Eqs. (36) and ((37)) are compared to Fig. 5e, f plots characteristics. For each system, the mean residence time relative error shows larger differences between components compared to their shock breakthrough time relative errors. The mismatch between theoretically derived metrics and results could be attributed to the assumptions upon which the theoretical estimations rely.

4. Theoretical performance analysis: hodographs

Multicomponent adsorption equilibrium theory allows the qualitative prediction of the equilibrium behaviour of isothermal, Langmuir isotherm-obeying systems. Glueckauf's work connected chromatographic theory and kinematic waves in a similar manner which resulted in the ability to predict multicomponent mixture dynamic behaviour. The foundation of the theory is the concept of coherence, which assumes that a front of multicomponent fluid is travelling along the column as a front of constant composition and can transition either as a continuous wave or a shock. For example, the feeding of an initially clean bed with a ternary mixture (two low-concentration adsorbable species with an inert carrier gas) generates a front travelling as a shock along the column, whose behaviour is critical during industrial operation.

In such a ternary mixture, the equilibrium of each adsorbable component depends on both components, which, also due to the coherence of waves, gives rise to the fundamental quadratic equation, Eq. (38):

$$\frac{\partial q_2}{\partial C_1}\left(\frac{\partial C_1}{\partial C_2}\right)^2 + \left(\frac{\partial q_2}{\partial C_2} - \frac{\partial q_1}{\partial C_1}\right)\frac{\partial C_1}{\partial C_2} - \frac{\partial q_1}{\partial C_2} = 0 \tag{38}$$

Glueckauf (1949) introduced an approach also presented by Ruthven (1984), which enables the binary Langmuir Isotherm analysis simplification by the introduction of the p_1, p_2 variables, where component 2 is assumed to be the strongly adsorbed. Therefore, b_2 is always larger than b_1 and Eq. (38) becomes:

$$p_1 = \frac{b_1 b_2 C_1}{b_2 - b_1} \tag{39}$$

$$p_2 = \frac{b_1 b_2 C_2}{b_2 - b_1} \tag{40}$$

$$\lambda = \frac{\partial C_1}{\partial C_2} \tag{41}$$

$$p_2\lambda^2 + (p_2 - p_1 - 1)\lambda - p_1 = 0 \tag{42}$$

Eq. (48) has two roots, where M is the positive and N is the negative. The transition of a system between the bed's initial and final (feed concentration) state can be described qualitatively on a hodograph plot of p_1 vs. p_2. This plot contains two points corresponding to the initial and final state of the bed respectively, as well as four straight lines passing through them, which correspond to the characteristic curves of p_1 and p_2 coherence equations (Eq. (42)) roots for each point, as follows:

$$p_1 = p_2 M - \frac{M}{1+M} \tag{43}$$

$$p_1 = p_2 N - \frac{N}{1+N} \tag{44}$$

Hodograph interpretation relies on 2 rules to predict the system's dynamic behaviour when transitioning from the bed's initial state to the bed's final (feed concentration) state (Glueckauf, 1949; Basmadjian, 1997):

1. One departs from the initial composition point on a positive root characteristic line and arrives at the final (feed) composition point on a negative root characteristic curve.

2. Whenever the more strongly adsorbed solute increases in concentration along the column we have a diffuse boundary while where the concentration of the more strongly adsorbed component decreases along the column we have a shock transition.

4.1. Hodograph theory case studies

The two simple rules of Hodograph Theory enable the prediction of binary mixture dynamic adsorption on a qualitative level. To this end, the adsorption of mixtures of dichloromethane with chloroform, dichloromethane with toluene and dichloromethane with acetone were studied at five different temperatures (T = 293 K–313 K) and two different bed states (clean and used) each. The API manufacturing site has an internal emissions limit for combined chloroform and dichloromethane of 18 ppm, so an initial concentration of 9 ppm per VOC was assumed for the used bed scenarios.

For each scenario, the coherence equation (Eq. (42)) is solved twice. Once for the initial state of the bed and once for the feed (final state). For the clean bed scenario, p_1 and p_2 are zero. Only one pair of M, N values are therefore computed and thus, 2 curves, corresponding to the feed state roots of the coherence equation are drawn on the clean bed hodographs (Figs. 10a, 11a, 12a). For the used bed scenario, the solution of the coherence equation gives 2 pairs of M, N values, corresponding to the four characteristic curves present on the used bed hodographs (Figs. 7b, 8b, 9b).

Table 11 shows the results of the coherence equation solution for the DCM-TCM system.

Table 12 shows the results of the coherence equation solution for the DCM-TOL system.

Table 13 shows the results of the coherence equation solution for the DCM-ACT system.

The clean bed hodographs of the dichloromethane–chloroform system are presented in Fig. 10a. In this system, TCM is the strongly adsorbed component and DCM is the weakly adsorbed component due to the larger Langmuir Isotherm parameter values of TCM compared to DCM. For the clean-bed scenario, 5 different temperatures were examined while the concentration remains the same at 250 ppm per VOC. For each temperature, the initial point is at the bottom left of the plot (0,0) while the feed point, corresponding to the final state of the bed, is moving closer to (0,0) with increasing temperature. That is due to the definitions of p_1, p_2 which include the Langmuir affinity coefficients. The Langmuir affinity coefficients are temperature dependant, as can be seen in Eq. (15), and more specifically, they decrease as temperature increases. Hence, the feed points on the hodograph for a specific system will be receiving smaller values with increasing temperature.

The used bed hodographs of the dichloromethane–chloroform system are shown in Fig. 10b. Here, the same five different temperatures

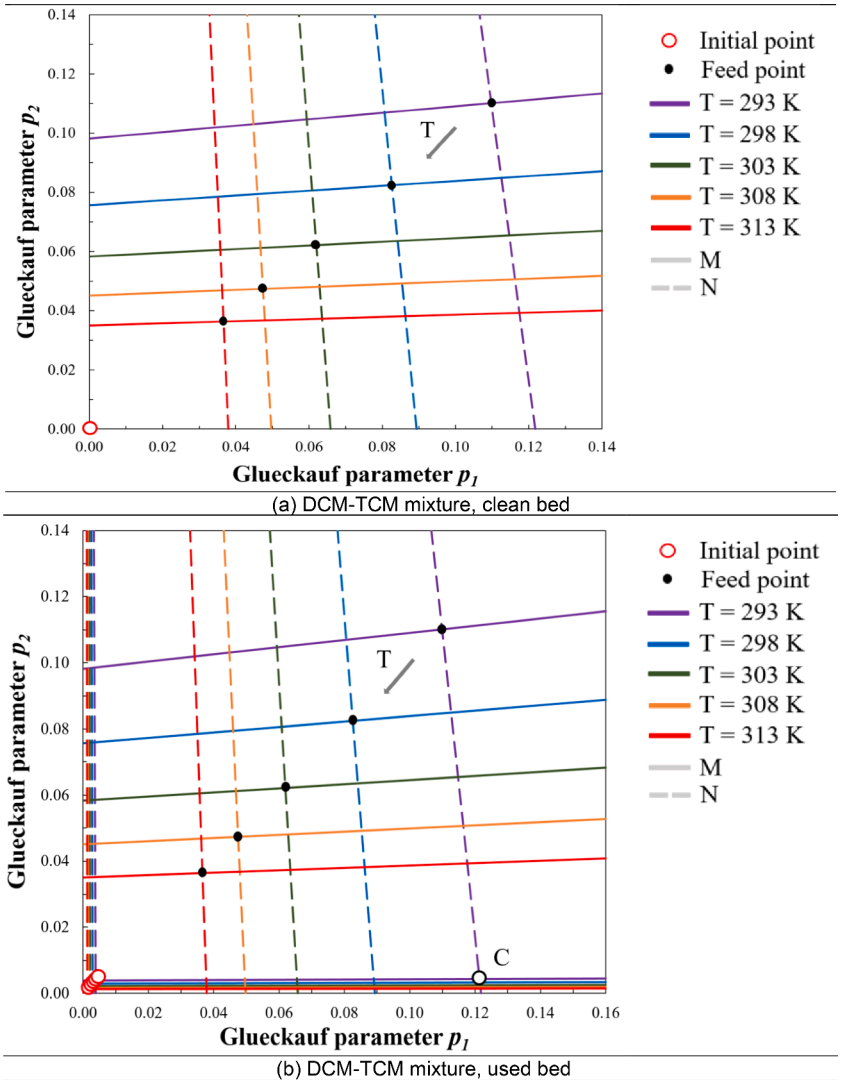

Fig. 10. Hodograph plots for the DCM-TCM system on a (a) clean and (b) used bed.

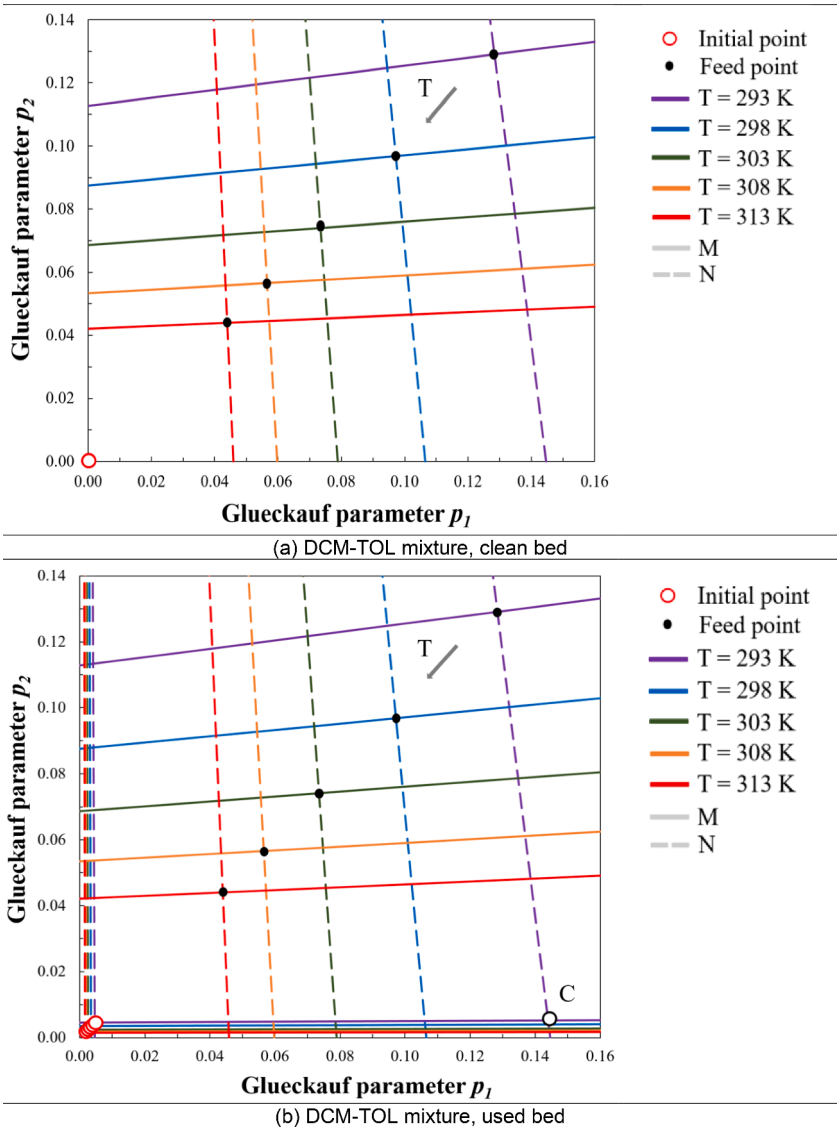

Fig. 11. Hodograph plots for the DCM-TOL system on a (a) clean and (b) used bed.

are explored but the beds have an initial concentration of 9 ppm per VOC while the feed concentration remains at 250 ppm per VOC. The gradual decline of the feed point values is due to the increased temperature, as in the clean bed cases. However, here, the predictive capabilities of hodograph theory can be displayed since there are now four lines on the p_1-p_2 plane, corresponding to the two pairs of roots of the coherence equation. As Rule 1 states, we depart from the initial point on a positive characteristic (M) line, therefore, for $T = 293$ K, we depart from the initial point on the continuous purple line and, we arrive at the feed point on the dashed purple line which corresponds to the negative characteristic. Therefore, if C is the point where the positive root characteristic (continuous purple line) and the negative root characteristic curve (dashed purple line) intersect, the route could be summarized as going to the feed point, from the initial point via C. Since the concentration of the strongly adsorbed component is decreasing due to an amount of it being adsorbed throughout the column, a shock transition occurs, as set out by Rule 2, and thus there is a sharp rise in the concentration of the weakly adsorbed component, which exits the column in a higher concentration compared to its inlet. The hodograph plots of all temperatures are interpreted in a similar manner. What is interestingly deducted by this method, is not only the prediction of the component to be displaced but also the observation that with rising operating temperature, the amount of displaced weakly adsorbed component decreases. This corroborates our simulations which clearly show that as temperature rises, the maximum concentration of the displaced component encountered at the column outlet declines.

Fig. 11a shows the clean bed hodographs of the dichloromethane–toluene system. In this system, toluene is the strongly adsorbed component and DCM is the weakly adsorbed component due to the smaller Langmuir Isotherm parameter values. For the clean bed scenario, 5 different temperatures were examined while the concentration remained the same at 250 ppm per VOC. For each temperature, the initial point is at the bottom left of the plot (0,0) while the feed point, corresponding to the final state of the bed, is moving closer to (0,0) with increasing temperature. That is due to the definitions of p_1, p_2 which include the Langmuir affinity coefficients. The Langmuir affinity coefficients are temperature dependant, as can be seen in Eq. (15), and more specifically, they decrease as temperature increases. Hence, the feed points on the hodograph for a specific system will be receiving smaller values with increasing temperature. This system has the lowest values on the hodograph for p_1 and p_2.

The used bed hodographs of the dichloromethane–toluene system are shown in Fig. 11b. Here, the same five different temperatures were explored but the beds had an initial concentration of 9 ppm per VOC

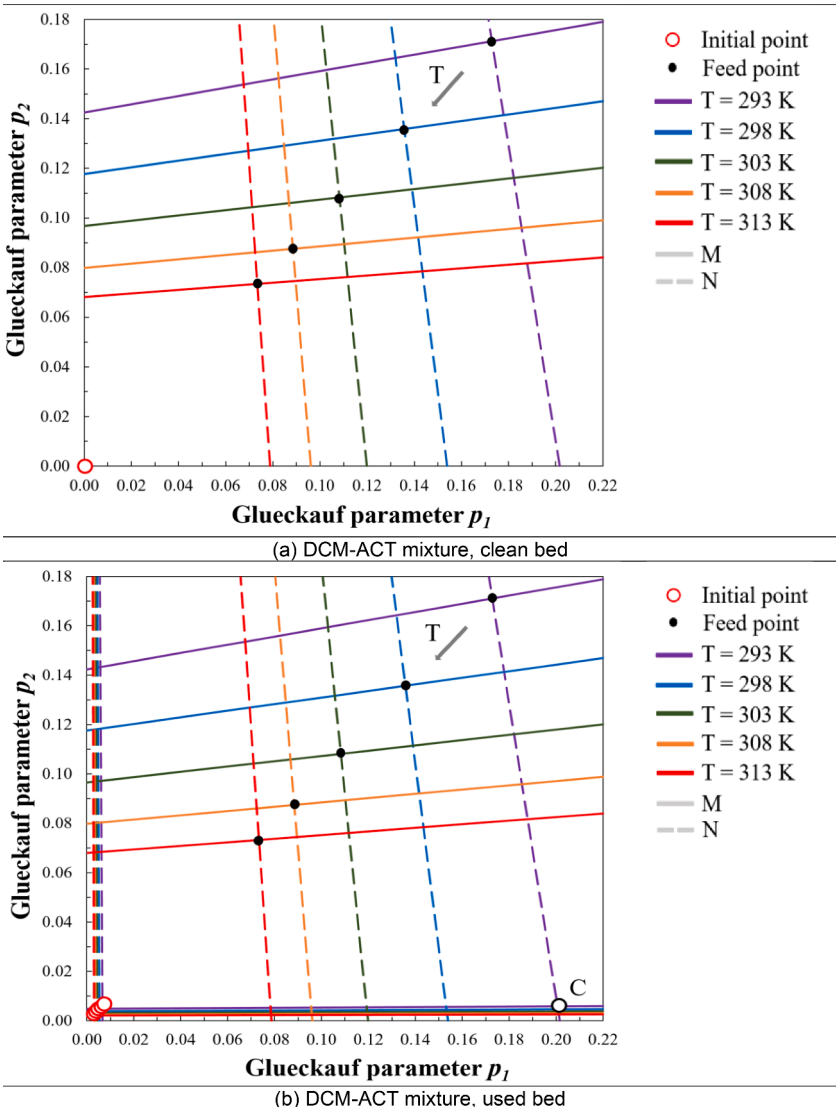

Fig. 12. Hodograph plots for the DCM-ACT system on a (a) clean and (b) used bed.

Table 11
Coherence equation solutions for the DCM-TCM system and clean/used bed.

System	T (K)	State	p_1	p_2	M	N
DCM-TCM (CLEAN BED)	293	Initial	0	0	–	–
		Feed	0.1100	0.1100	9.1830	−0.1090
	298	Initial	0	0	–	–
		Feed	0.0826	0.0824	12.2110	−0.0821
	303	Initial	0	0	–	–
		Feed	0.0620	0.0622	16.1340	−0.0617
	308	Initial	0	0	–	–
		Feed	0.0474	0.0474	21.1300	−0.0473
	313	Initial	0	0	–	–
		Feed	0.0366	0.0363	27.5340	−0.0365
DCM-TCM (USED BED)	293	Initial	0.0039	0.0039	254.9140	−0.0039
		Feed	0.1100	0.1100	9.1830	−0.1086
	298	Initial	0.0029	0.0029	336.7910	−0.0029
		Feed	0.0826	0.0824	12.2109	−0.0820
	303	Initial	0.0022	0.0022	446.3244	−0.0022
		Feed	0.0619	0.0622	16.1343	−0.0617
	308	Initial	0.0017	0.0017	585.6890	−0.0017
		Feed	0.0474	0.0474	21.1409	−0.0473
	313	Initial	0.0013	0.0013	763.3631	−0.0013
		Feed	0.0365	0.0363	27.5339	−0.0365

Table 12
Coherence equation solutions for the DCM-TOL system and clean/used bed.

System	T (K)	State	p_1	p_2	M	N
DCM-TOL (CLEAN BED)	293	Initial	0	0	–	–
		Feed	0.1284	0.1291	7.8664	−0.1264
	298	Initial	0	0	–	–
		Feed	0.0972	0.0968	10.4278	−0.0962
	303	Initial	0	0	–	–
		Feed	0.0734	0.0740	13.5667	−0.0731
	308	Initial	0	0	–	–
		Feed	0.0566	0.0565	17.7338	−0.0564
	313	Initial	0	0	–	–
		Feed	0.0440	0.0440	22.7682	−0.0439
DCM-TOL (USED	293	Initial	0.0046	0.0045	218.7553	−0.0046
		Feed	0.1283	0.1291	7.8664	−0.1263
	298	Initial	0.0034	0.0035	285.4714	−0.0034
		Feed	0.0972	0.0968	10.4278	−0.0962
	303	Initial	0.0025	0.0023	417.9689	−0.0025
		Feed	0.0734	0.0740	13.5666	−0.0731
	308	Initial	0.0020	0.0018	535.7988	−0.0020
		Feed	0.0566	0.0565	17.7338	−0.0564
	313	Initial	0.0015	0.0014	681.1179	−0.0015
		Feed	0.0440	0.0440	22.7682	−0.0439

while the feed concentration remained at 250 ppm per VOC. The gradual decline of the feed point values is due to the increased temperature, as in the clean bed cases. According to Rule 1, departure from the initial point occurs on a positive characteristic (M) line, therefore, for $T = 293$ K we depart from the initial point on the continuous purple line and, we arrive at the feed point on the dashed purple line which corresponds to the negative characteristic. Thus, if C is the point where the positive root characteristic (continuous purple line) and the negative root characteristic curve (dashed purple line) intersect, the route could be summarized as going to the feed point, from the initial point via C. Since the concentration of the strongly adsorbed component is decreasing due to an amount of it being adsorbed throughout the column, a shock transition occurs, as set out by Rule 2, and thus a sharp rise in the concentration of the weakly adsorbed component occurs, leading to its exit in a higher concentration compared to its inlet. The hodograph plots of all temperatures are interpreted in a similar manner. What is interestingly deducted by this method, is not only the prediction of the component to be displaced, but also the observation that with rising operating temperature, the amount of displaced weakly adsorbed component decreases.

Fig. 12a shows the clean bed hodographs of the dichloromethane–acetone system. In this system, acetone is the strongly adsorbed component and DCM is the weakly adsorbed component due to the smaller Langmuir Isotherm parameter values. For the clean bed scenario, five different temperatures were examined while the concentration remained the same at 250 ppm per VOC. For each temperature, the initial point is at the bottom left of the plot (0,0) while the feed point, corresponding to the final state of the bed, is moving closer to (0,0) with increasing temperature. That is due to the definitions of p_1, p_2 which include the Langmuir affinity coefficients. The Langmuir affinity coefficients are temperature dependant, as can be seen in Eq. (15), and more specifically, they decrease as temperature increases. Hence, the feed points on the hodograph for a specific system will be receiving smaller values with increasing temperature. This system demonstrates the highest p_1-p_2 values compared to the others.

The used bed hodographs of the dichloromethane–acetone system are shown in Fig. 12b, for five different temperatures and an initial bed concentration of 9 ppm per VOC. The feed concentration remained at 250 ppm per VOC. The gradual decline of the feed point values is due to the increased temperature, as in the clean bed cases. According to Rule 1, departure from the initial point occurs on a positive characteristic (M) line, therefore, for $T = 293$ K we depart from the initial point on the

Table 13
Coherence equation solutions for the DCM-ACT system and clean/used bed.

System	T (K)	State	p_1	p_2	M	N
DCM-ACT (CLEAN BED)	293	Initial	0	0	–	–
		Feed	0.1729	0.1712	6.0186	−0.1678
	298	Initial	0	0	–	–
		Feed	0.1358	0.1358	7.4963	−0.1334
	303	Initial	0	0	–	–
		Feed	0.1082	0.1082	9.3459	−0.1070
	308	Initial	0	0	–	–
		Feed	0.0884	0.0875	11.5227	−0.0877
	313	Initial	0	0	–	–
		Feed	0.0734	0.0734	13.7035	−0.0730
DCM-ACT (USED BED)	293	Initial	0.0066	0.0049	200.8863	−0.0066
		Feed	0.1729	0.1712	6.0186	−0.1678
	298	Initial	0.0053	0.0039	250.6769	−0.0053
		Feed	0.1358	0.1358	7.4963	−0.1334
	303	Initial	0.0043	0.0032	308.3027	−0.0043
		Feed	0.1082	0.1082	9.3459	−0.1070
	308	Initial	0.0035	0.0026	373.5492	−0.0035
		Feed	0.0884	0.0875	11.5227	−0.0876
	313	Initial	0.0029	0.0022	445.5996	−0.0029
		Feed	0.0733	0.0733	13.7034	−0.0729

continuous purple line and, we arrive at the feed point on the dashed purple line which corresponds to the negative characteristic. Thus, if C is the point where the positive root characteristic (continuous purple line) and the negative root characteristic curve (dashed purple line) intersect, the route could be summarized as going to the feed point, from the initial point via C. Since the concentration of the strongly adsorbed component is decreasing due to an amount of it being adsorbed throughout the column, a shock transition occurs, as set out by Rule 2, and thus a sharp rise in the concentration of the weakly adsorbed component occurs, leading to its exit in a higher concentration compared to its inlet. The hodograph plots of all temperatures are interpreted in a similar manner. It is observed that with rising operating temperature, the amount of displaced dichloromethane decreases thus corroborating our results shown in Fig. 4b, where the temperature sensitivity analysis of the same system clearly shows a decline in the maximum DCM concentration at the column outlet with rising temperature.

5. Conclusions

Primary pharmaceutical manufacturing is heavily reliant on solvents, thus exacerbating effects on the environment and public health due to VOC emissions. Due to growing environmental concerns and corresponding ever-tightening regulations, the pharmaceutical industry focuses on drastic climate impact minimisation and profitability improvement via process optimisation. End-of-pipe mitigation solutions are often selected because solvent substitution may not be preferable (if at all possible), since it entails great uncertainty in regard to regulatory approvals. Adsorption is an industrially established, reliable and widespread VOC waste capture method, which however has known flexibility limitations and poses operational efficiency challenges. Despite the abundance of comprehensive modelling and experimental studies in the literature, research on pharma-relevant, multicomponent VOC mixture adsorption, breakthrough order and outlet concentration evolution has not focused on plantwide efficiency considerations (Tzanakopoulou et al., 2021, 2022). Published studies are scarce for such mixtures under industrially relevant conditions, in which larger length- and time-scales render experiments arduous and/or prohibitively expensive, thus accentuating the value of modelling to aid operational decisions for production facilities.

The present paper first reviews several literature studies in order to establish a database of pharma-relevant solvent (acetone, chloroform, dichloromethane, toluene) Langmuir Isotherm parameters for adsorption on activated carbon materials through parameter estimation. In several studies, Langmuir Isotherm parameter values required for simulations may have not been accurately estimated and/or explicitly reported, obstructing the validation of extremely useful experiments. Our parameter estimation results are very promising in the majority of cases and emphasise the enormous variation in certain parameter values (e.g. maximum adsorption capacity of materials, Langmuir affinity coefficient), which can be as high as 2–4 orders of magnitude, respectively. This considerable (and alarming, for modelling purposes) uncertainty is a reflection of the extremely wide range of activated carbon (AC) material types, microstructures, processing protocols and physicochemical characteristics (many of which may similarly have not been quantified or comprehensively reported, as beyond the purpose).

This paper continues to demonstrate the development and application of a one-dimensional in space, multicomponent, nonisothermal adsorption model to highlight the complex phenomena taking place inside pharma VOC adsorption columns, considering axial dispersion in the gas phase as well as the Linear Driving Force model for solid phase mass transport. The continuous feeding of multicomponent VOC mixtures to the adsorption column results in quickly and irregularly saturated beds. Thus, establishing a clear image for VOC breakthrough relationships is essential. Dynamic simulations of VOC adsorption for three industrially critical binary systems (namely mixtures of dichloromethane with acetone, toluene and chloroform) revealed that the VOC breakthrough order off the industrial activated carbon bed is: dichloromethane (DCM), then acetone, toluene and chloroform, i.e. trichloromethane (TCM). Our gPROMS dynamic model is validated against experimental data by Talmoudi et al. (2018).

Furthermore, the temperature sensitivity analysis via dynamic simulation revealed that higher operating temperatures lead to shorter breakthrough times, while the effect of bed porosity on binary mixture behaviour is more complex, and system-specific. Theoretical prediction formulas from the literature (mean residence and shock breakthrough times, Eqs. (32) and (34) have been compared to our gPROMS dynamic simulation results, showing that the former (albeit originally derived for single-component, isothermal conditions) can provide quick, useful estimates to inform industrial operation, before committing resources in pursuit of the latter. Discrepancies of max. 30% are observed for all but one (DCM) components in most cases, implying the said Eqs. are extremely useful before undertaking detailed dynamic simulations. Dichloromethane (DCM), however, yields higher discrepancies (80%) in the said comparison, indicating that order-of-magnitude estimates are still possible, but dynamic simulation is very much justified for VOC capture intensification, especially as it is the first gas to break through.

Axial dispersion is accounted for in our model in Eqs. (2) and (3). Fixed bed adsorbers suffer from their tendency to develop axial dispersion, a phenomenon which reduces process efficiency (Ruthven, 1984) as it prevents adsorbates from diffusing into the adsorbent material due to axial mixing and therefore could have an influence on breakthrough completion time. Kinetic effects have been ignored in accordance with literature, but must be revisited in subsequent studies. Moreover, pressure drop is modelled via Ergun's Equation, considered preferable compared to other methods due to its direct dependence on bed voidage (Ruthven, 1984). Pressure directly affects the adsorption of contaminants on activated carbon and can increase the time needed for adsorbent saturation (thus breakthrough completion), especially in larger beds. Numerical dispersion is another potential cause of discrepancies: when numerical discretization is applied to analyse physical processes, even if many of them are modelled by nondispersive PDEs, typically a small dispersion emerges in results (Griffiths, 2016).

Finally, hodograph theory has been applied to demonstrate the prediction capabilities of this simple, fast, and yet first-principles consistent concept, enabling binary mixture dynamic behaviour predictions. Hodograph theory results corroborate our simulations not only regarding the order of VOC affinity to the bed, but also in that with rising temperature the maximum concentration of the weak component at the column outlet decreases. This paper paves the way for detailed technoeconomic optimisation of multicomponent, nonisothermal VOC adsorption scheduling.

CRediT authorship contribution statement

Vasiliki E. Tzanakopoulou: Conceptualization, Methodology, Software, Writing – review & editing. **Michael Pollitt:** Conceptualization, Writing – review & editing, Supervision. **Daniel Castro-Rodriguez:** Conceptualization, Writing – review & editing, Supervision. **Alexandra Costa:** Conceptualization, Writing – review & editing, Supervision. **Dimitrios I. Gerogiorgis:** Conceptualization, Methodology, Writing – review & editing, Funding acquisition, Supervision.

Declaration of Competing Interest

None.

Data availability

Data will be made available on request.

Acknowledgements

The authors gratefully acknowledge the SRPe-NMIS IDP PhD Scholarship awarded to V.T., as well as a recent Royal Society Short Industrial Fellowship (2020–22) awarded to D.I.G. Furthermore, we gratefully acknowledge financial support from the Engineering and Physical Sciences Research Council (EPSRC UK) and UK Research & Innovation (UKRI), under the auspices of an ongoing grant (RAPID: ReAltime Process ModellIng & Diagnostics - Powering Digital Factories, EP/V028618/1).

References

Akbar, M., Irohara, T., 2018. Scheduling for sustainable manufacturing: a review. J. Clean. Prod. 205, 866–883.
Basmadjian, D., 1997. The Little Adsorption Book: A Practical Guide for Engineers and Scientists. CRC Press.
Borkar, C., Tomar, D., Gumma, S., 2010. Adsorption of dichloromethane on activated carbon. J. Chem. Eng. Data 55 (4), 1640–1644.
Chiang, Y.C., Chiang, P.C., Huang, C.P., 2001. Effects of pore structure and temperature on VOC adsorption on activated carbon. Carbon 39 (4), 523–534.
Chuang, C.L., Chiang, P.C., Chang, E.E., 2003. Modelling VOCs adsorption onto activated carbon. Chemosphere 53 (1), 17–27.
Constable, D.J.C., Jimenez-Gonzalez, C., Henderson, R.K., 2007. Perspective on solvent use in the pharmaceutical industry. Org. Process Res. Dev. 11 (1), 133–137.
Das, D., Gaur, V., Verma, N., 2004. Removal of volatile organic compound by activated carbon fiber. Carbon 42 (14), 2949–2962.
Delage, F., Pré, P., Le Cloirec, P., 2000. Mass transfer and warming during adsorption of high concentrations of VOCs on an activated carbon bed: experimental and theoretical analysis. Environ. Sci. Technol. 34 (22), 4816–4821.
Delgado, J.M.P.Q., 2006. A critical review of dispersion in packed beds. Heat Mass Transf. 42 (4), 279–310.
EEA, 2019. Emissions of Main Air Pollutants by Sector in EEA. EEA. www.eea.europa.eu/data-and-maps.
Gales, L., Mendes, A., Costa, C., 2000. Hysteresis in the cyclic adsorption of acetone, ethanol and ethyl acetate on activated carbon. Carbon 38, 1083–1088.
Gales, L., Mendes, A., Costa, C., 2003. Recovery of acetone, ethyl acetate and ethanol by thermal pressure swing adsorption. Chem. Eng. Sci. 58 (23), 5279–5289.
Gerogiorgis, D.I., Barton, P.I., 2009. Steady-state optimization of a continuous pharmaceutical process. Comput. Aided Chem. Eng. 27, 927–932.
Gerogiorgis, D.I., Jolliffe, H.G., 2015. Continuous pharmaceutical process engineering and economics Investigating technical efficiency, environmental impact and economic viability. Chim. Oggi - Chem. Today 33 (6), 29–32.
Giraudet, S., Pré, P., Le Cloirec, P., 2009. Modeling the heat and mass transfers in temperature-swing adsorption of volatile organic compounds onto activated carbons. Envir. Sci. Tech. 43 (4), 1173–1179.
Giraudet, S., Pré, P., Le Cloirec, P., 2010. Modeling the temperature dependence of adsorption equilibriums of VOC(s) onto activated carbons. J. Environ. Eng. 136 (1), 103–111.
Giret, A., Trentesaux, D., Prabhu, V., 2015. Sustainability in manufacturing operations scheduling: a state of the art review. J. Manuf. Syst. 37, 126–140.
Glueckauf, E., 1949. The general theory of two solutes following non-linear isotherms. Discuss. Faraday Soc. 7, 12–25.
Griffiths, G., 2016. Dissipation and dispersion. Numerical Analysis Using R: Solutions to ODEs and PDEs. Cambridge University Press, Cambridge, pp. 264–284.
Jolliffe, H.G., Gerogiorgis, D.I., 2015. Plantwide design and economic evaluation of two Continuous Pharmaceutical Manufacturing (CPM) cases: Ibuprofen and artemisinin. Comput. Aided Chem. Eng. 37, 2213–2218.
Jolliffe, H.G., Gerogiorgis, D.I., 2017. Technoeconomic optimisation and comparative environmental impact evaluation of continuous crystallisation and antisolvent selection for artemisinin recovery. Comput. Chem. Eng. 103, 218–232.
Kalender, M., Akosman, C., 2015. Removal of chlorinated volatile organic compounds by fixed bed adsorption technique: adsorption equilibrium and breakthrough analyses. Rom. Biotechnol. Lett. 20 (2), 10245.
Kim, S.J., Cho, S.Y., Kim, T.Y., 2002. Adsorption of chlorinated volatile organic compounds in a fixed bed of activated carbon. Korean J. Chem. Eng. 19 (1), 61–67.
Knox, J.C., Ebner, A.D., LeVan, M.D., et al., 2016. Limitations of breakthrough curve analysis in fixed-bed adsorption. Ind. Eng. Chem. Res. 55 (16), 4734–4748.
Kotchine, N.E., 1926. Sur la théorie des ondes de choc dans un fluide. Rend. Circ. Mat. Palermo Ser. 2 50, 305–344.
Krishna, R., Van Baten, J.M., 2012. Investigating the validity of the Bosanquet formula for estimation of diffusivities in mesopores. Chem. Eng. Sci. 69 (1), 684–688.
Lemus, J., Martin-Martinez, M., Palomar, J., et al., 2012. Removal of chlorinated organic volatile compounds by gas phase adsorption with activated carbon. Chem. Eng. J. 211-212, 246–254.
Li, Z., Li, Y., Zhu, J., 2021. Straw-based activated carbon: optimization of the preparation procedure and performance of volatile organic compounds adsorption. Materials 14 (12), 3284.
Logan, D.A., 1997. Estimating physical properties for control equipment design. Environ. Prog. 16 (4), 237–244.
Manjare, S.D., Ghoshal, A.K., 2006. Studies on adsorption of ethyl acetate vapor on activated carbon. Ind. Eng. Chem. Res. 45 (19), 6563–6569.
Meng, F., Song, M., Wei, Y., et al., 2019. The contribution of oxygen-containing functional groups to the gas-phase adsorption of volatile organic compounds with different polarities onto lignin-derived activated carbon fibers. Environ. Sci. Pollut. Res. Int. 26 (7), 7195–7204.
NIST, 2021. NIST Chemistry WebBook (Linstrom, P.J., Mallard, W.G., Eds.), NIST Standard Reference Database Number 69, National Institute of Standards and Technology (NIST), Gaithersburg, MD 20899, USA.
Pré, P., Delage, F., Le Cloirec, P., 2002. A model to predict the adsorber thermal behavior during treatment of volatile organic compounds onto wet activated carbon. Environ. Sci. Technol. 36 (21), 4681–4688.
Ramirez, D., Qi, S., Rood, M.J., et al., 2005. Equilibrium and heat of adsorption for organic vapors and activated carbons. Environ. Sci. Technol. 39 (15), 5864–5871.
Ruthven, D.M., 1984. Principles of Adsorption and Adsorption Processes. Wiley, New York.
Saleh, T.A., Alhooshani, K.R., Abdelbassit, M.S.A., 2015. Evaluation of AC/ZnO composite for sorption of dichloromethane, trichloromethane and carbon tetrachloride: kinetics and isotherms. J. Taiwan Inst. Chem. Eng. 55, 159–169.
Sircar, S., Hufton, J.R., 2000. Why does the LDF model for adsorption kinetics work. Adsorption 6 (2), 137–147.
Suzuki, M., 1990. Adsorption Engineering. Elsevier, Amsterdam.
Talmoudi, R., AbdelJaoued, A., Chahbani, M.H., et al., 2018. Dynamic study of VSA and TSA processes for VOCs removal from air. Int. J. Chem. Eng. 2018, 1–15.
Tefera, D.T., Hashisho, Z., Philips, J.H., et al., 2014. Modeling competitive adsorption of mixtures of volatile organic compounds in a fixed-bed of beaded activated carbon. Environ. Sci. Technol. 48 (9), 5108–5117.
Tefera, D.T., Lashaki, M.J., Fayaz, M., et al., 2013. Two-dimensional modeling of volatile organic compounds adsorption onto beaded activated carbon. Environ. Sci. Technol. 47 (20), 11700–11710.
Tsai, J.H., Chiang, H.M., Huang, G.Y., et al., 2008. Adsorption characteristics of acetone, chloroform and acetonitrile on sludge-derived adsorbent, commercial granular activated carbon and activated carbon fibers. J. Hazard. Mater. 154 (1), 1183–1191.
Tzanakopoulou, V.E., Castro-Rodriguez, D., Gerogiorgis, D.I., 2021. Process modelling and simulation of VOC recovery from pharmaceutical gas emission streams. Comput. Aided Chem. Eng. 50, 717–723.
Tzanakopoulou, V.E., Costa, A., Castro-Rodriguez, D., Gerogiorgis, D.I., 2022. Multicomponent, nonisothermal VOC adsorption modelling for pharmaceutical effluent purification: effect of operating conditions on bed performance. Comput. Aided Chem. Eng. 51, 331–336.
Vuong, F., Chauveau, R., Grevillot, G., et al., 2016. Predicting the lifetime of organic vapor cartridges exposed to volatile organic compound mixtures using a partial differential equations model. J. Occup. Environ. Hyg. 13 (9), 675–689.
Xiong, Y., Zhou, J., Xing, Z., et al., 2021. Cancer risk assessment for exposure to hazardous volatile organic compounds in Calgary, Canada. Chemosphere 272, 129650.
Yang, X., Yi, H., Tang, X., et al., 2018. Behaviors and kinetics of toluene adsorption-desorption on activated carbons with varying pore structure. J. Environ. Sci. 67, 104–114.
Yanxu, L., Jiangyao, C., Yinghuang, S., 2008. Adsorption of multicomponent volatile organic compounds on semi-coke. Carbon 46 (6), 858–863.
Yao, X., Liu, Y., Li, T., et al., 2020. Adsorption behavior of multicomponent volatile organic compounds on a citric acid residue waste-based activated carbon: experiment and molecular simulation. J. Hazard. Mater. 392, 122323.
Zhou, C., Zhou, K., Li, H., et al., 2021. Pressure swing adsorption properties of activated carbon for methanol, acetone and toluene. Chem. Eng. J. 413, 127384.